Swi4-dependent *SWI4* transcription couples cell size to cell cycle commitment.

Pooja Goswami[1,#,‡], Abhishek Ghimire[1,#], Carleton Coffin[1], Jing Cheng[2,††], Jasmin Coulombe-Huntington[3†], Ghada Ghazal[3], Yogitha Thattikota[2¶], Sylvain Tollis[3,$,*], Mike Tyers[2,*] and Catherine A. Royer[1,*]

[1]Department of Biological Sciences, Rensselaer Polytechnic Institute, Troy, NY 12180, USA

[2]Program in Molecular Medicine, Peter Gilgan Centre for Research and Learning, The Hospital for Sick Children, Toronto, ON M5G 0A4, Canada

[3]Institute of Research in Immunology and Cancer, University of Montreal, QCH3T1J4, Quebec, Canada

[‡]Current address: Department of Neurology, Brain Science Institute, Johns Hopkins University School of Medicine, Baltimore MD 21205 USA

[†]Current address: Department of Bioengineering, McGill University, Montreal, H3A 0E9, Quebec, Canada

[¶]Current address: Montreal Neurological Institute, McGill University, Montréal, H3A 2B4, Québec, Canada;

[$]Current address: Institute of Biomedicine, School of Medicine, Faculty of Health Sciences, University of Eastern Finland, Joensuu, 70211 Kuopio, Finland

#These authors contributed equally to the work.
*- To whom correspondence should be addressed:
sylvain.tollis@uef.fi, mike.tyers@sickkids.ca, royerc@rpi.edu,

Abstract

Growth-dependent accumulation of the SBF transcription factor, composed of Swi4 and Swi6, occurs as cells approach the G1/S transition (Start) in budding yeast. Here we measure size-dependence of Swi4 protein copy number under different genetic contexts using the scanning number and brightness particle counting technique. Mutation of SBF binding sites in the *SWI4* promoter or disruption of SBF activation resulted in ~33-50% decrease in the rate of Swi4 accumulation with cell size. Ectopic inducible expression of Swi4 in G1 phase cells increased production of Swi4 from the endogenous promoter and concomitantly upregulated transcription of the G1/S regulon. Despite the potential for Swi4 positive feedback, Swi4 accumulated linearly through G1 phase unless the Whi5 transcriptional repressor was inactivated. A threshold level of 190 Swi4 molecules titrating SBF binding sites in G1/S promoters predicted the effects of nutrients, ploidy, and G1/S regulatory mutations on cell size. These results reveal how transcription factor auto-production can contribute to a cell state transition.

Introduction

The G1/S transition is controlled at the transcriptional level in organisms from yeast to humans (1, 2). In budding yeast, this transition (termed Start) is activated by the SBF and MBF transcription factor (TF) complexes (3), which govern expression of the ~200 genes in the G1/S regulon. These complexes comprise the same Swi6 activator subunit, and distinct DNA binding subunits, Swi4 and Mbp1, respectively. SBF and MBF bind to target sites, SCB and MCB (3–5), present in promoters of the G1/S regulon. The timing of the G1/S transition, as activated by SBF and MBF, relative to cell growth determines cell size at Start. While deletion of MBP1 in cells grown on rich nutrients does not significantly increase cell size, *swi4Δ* mutants are extremely large, demonstrating that under these conditions, SBF is the dominant transcriptional activator of Start (6). Transcriptional activation by SBF is repressed during G1 phase by Whi5 (7). The SBF-Whi5 complex is phosphorylated on multiple sites by the Cln-Cdc28 cyclin-dependent kinases in late G1, resulting in dissociation and Whi5 export from the nucleus, which is the earliest molecular indicator of Start (8, 9). Deletion of the upstream G1 cyclin Cln3 individually leads to very large cells (10), while the triple *CLN1/2/3* deletion or inactivation of Cdc28 causes arrest at Start (11–13). Importantly, *CLN1/2* are key genes in the G1/S regulon, and form part of a phosphorylation-driven positive feedback loop that serves to sharpen the Start transition (14) Deletion of WHI5 causes a small cell size phenotype that is epistatic to deletion of *SWI4* (7), underscoring the central role of SBF at Start.

We have shown previously by scanning Number and Brightness (sN&B) microscopy that the absolute copy numbers of Swi4 and Mbp1 in early G1 phase are limiting with respect to their ~200 target G1/S promoters (6). Copy numbers of all SBF/MBF subunits increase during G1 to levels that eventually saturate G1/S promoters, representing an important potential determinant of Start activation. In particular, Swi4 copy number is much lower than that of Mbp1, Swi6 or Whi5 in small cells but increases ~5-6-fold throughout G1 phase, leading to a doubling of its nuclear concentration. In contrast, as determined by sN&B, absolute protein copy number accumulation of Swi6, Mbp1 and Whi5 scales linearly with growth, with concomitantly constant nuclear concentrations in G1 phase. The measurement of Whi5 concentration is controversial since relative measurements by epifluorescence microscopy suggest that Whi5 is diluted as calls grow (15, 16), although this signal reduction may be due to photobleaching and other effects (17). The positive differential accumulation of Swi4 with respect to growth and to the other G1/S TFs raises the key question of how the expression of Swi4 during G1 phase is regulated.

An upstream activating sequence (UAS) in the SWI4 promoter contains several SCB/MCB sites, as well as an Early Cell Cycle Box (ECB) (18). The Mcm1 transcriptional activator, which binds the ECB (19), contributes to Swi4, Swi6 and Mbp1 production (20, 21). Deletion of 140 base pairs corresponding to this UAS causes a 10-fold decrease in Swi4 production (18). Deletion of SWI6 also decreases Swi4 levels and abrogates its cyclic production (18), demonstrating a contribution from the SCB/MCB sites to Swi4 expression. Furthermore, genome-wide CHIP-seq experiments demonstrated a physical interaction of Swi4 with its own promoter (4, 21). Based on these observations, Swi4-dependent Swi4 expression has been postulated (4, 18, 21, 22). However, this mechanism has never been quantitatively established nor its potential role at Start evaluated. Moreover, if indeed Swi4 regulates SWI4 expression, it is unknown whether this effect is mediated by both SBF and MBF.

In this study we investigated Swi4-dependent *SWI4* transcription and quantified its contribution to Swi4 protein production. Using the sN&B fluorescence microscopy particle counting technique (6), we found that deletion or mutation of different combinations of the SCB/MCB sites in the *SWI4* promoter resulted in a ~33-46% decrease in the rate of accumulation of Swi4 copy number with respect to growth. Disruption of phosphorylation of the SBF-Whi5 repressor complex – but not *MBP1* deletion - resulted in a ~50% decrease in Swi4 accumulation rate, further implicating SBF in its own production. Ectopic expression of Swi4 from a β-estradiol

(BE2)-dependent promoter led to a BE2-dependent increase of Swi4 expression from the endogenous promoter, which was accompanied by upregulation of genes in the G1/S regulon. A threshold of 190 Swi4 copies appeared to be required for Start and suggested that titration of G1/S promoters may account for the timing of Start in various environmental and genetic contexts. Together, these results demonstrate that SBF-mediated *SWI4* transcription accelerates the G1/S transition.

Results

Swi4 binding sites in the SWI4 promoter contribute to Swi4 protein expression

To test the role of Swi4 in its own production we used 2-photon (2p) sN&B particle counting to determine absolute values of intracellular concentrations of fluorescently tagged proteins (6). We measured the absolute nuclear concentration of Swi4 fused to fast maturing-monomeric GFPmut3 (hereafter referred to as Swi4-GFP for simplicity) expressed from its endogenous locus in asynchronously growing single cells grown in SC+2% glucose medium (6). Individual cell sizes were determined from the single cell images and the nuclear volume was assumed to be 1/7th of the total cell volume (23). Swi4 nuclear copy number was calculated as the product of the average nuclear concentration and the nuclear volume. Since Swi4 exits the nucleus sometime after budding but before mitosis (6), the measured cells with nuclear Swi4 were either in G1 or S-phase.

We compared Swi4-GFP protein copy numbers as a function of cell size in asynchronous populations of otherwise wild-type (WT) Swi4-GFP cells to Swi4 copy numbers in Swi4-GFP strains bearing various deletions or mutations in the *SWI4* promoter region (Figs. 1, S1, Table S1). In addition to three clustered central SCB/MCB promoter sites (termed site C in Fig. 1) situated ~30 bp upstream of the ECB site documented previously (18), we identified two other putative SCB sites, one situated ~1200 bp (termed site U) and the other ~270 bp upstream of the *SWI4* ORF (termed site D) that could potentially contribute to *SWI4* expression.

Deletion of the central region harboring two MCB sites and one SCB site (a total of 70 bp deleted, C delete) decreased the rate of accumulation of Swi4-GFP protein copy number with respect to cell size (*dSwi4/fL*) by 33% compared to WT, while mutation (as opposed to deletion) of the same central sites (C mutations) resulted in a slightly larger (37%) decrease (Fig. 2A, Table 1, Table S1). This same mutation of the central promoter region, together with mutation of the downstream SCB site (C+D mutations, Fig. 1B) also decreased Swi4-GFP accumulation (~38%), while additional mutation of the upstream SCB site (C+D+U mutations, Fig. 1B) decreased Swi4 accumulation even further (46%) (Fig. 2B, Table 1). These results establish that the MCB/SCB sites in the Swi4 promoter are responsible collectively for about half of total Swi4 protein expression in G1-S phase haploid cells. In heterozygous *SWI4/SWI4-GFP* diploid cells, the rate of accumulation of Swi4 nuclear copy number (per haploid genome) with respect to size was 58% lower than in haploids, while the deletion of the central promoter on the remaining allele expressing Swi4-GFP lowered the accumulation rate even further (67%, Table 1, Fig. S2). Note that total Swi4 accumulation rate with respect to size (i.e., inferring the same rate for GFP-labeled and unlabeled Swi4) in heterozygous *SWI4/SWI4-GFP* diploids corresponds to only a 16% increase compared to haploids, even though there are two *SWI4* loci and twice as many G1/S TF target sites in diploids. We do not know the basis for this reduced Swi4 accumulation in diploids, but it may help explain why diploids are approximately twice as large a haploids.

In agreement with our previously published model, in which Swi4 dosage is a limiting factor for cell cycle commitment (6), deletions or mutations of the various MCB/SCB sites in the SWI4 promoter in haploid cells led to a modest large size phenotype, as assessed by Coulter counter measurements (Figs. S1, S3A-C, S4, Table S2). The average size, as derived from the images of cells exhibiting nuclear Swi4-GFP, was also larger for the promoter mutants compared to WT cells (Fig. S1, Table 2). This phenotype was reduced in SWI4/*SWI4-GFP* heterozygous diploids, where the mean size for the *SWI4*/*C delete:SWI4-GFP* heterozygous diploid was ~2fL larger than WT diploid (Fig. S3, Table S2). These results show that mutations that diminish the rate of Swi4 production led to a delay in Start, and a larger cell size.

Cln3-Cdc28 mediated phosphorylation is required for Swi4 accumulation

We next evaluated the Cdc28-dependence of Swi4 accumulation. Chemical inhibition of kinase activity in a strain expressing an analog sensitive Cdc28, *CDC28-as1* (24), with 10 mM of the inhibitor, 1-(tert-butyl)-3-(naphthalene-1-methyl)-1H-pyrazolo [3,4-d] pyrimidine-4-amine (1-NM-PP-1) resulted in a large decrease in Swi4-GFP copy number accumulation (56%) with respect to cell size (Fig. 2C, Table 1). Hence, Cdc28 kinase activity drives approximately half of Swi4 accumulation in G1 phase. The rate of Swi4-GFP accumulation in absence of the inhibitor was slightly lower (23%) than for WT cells, perhaps due to impaired kinase activity of the Cdc28-as1 protein. To exclude the possible indirect contribution of Cdc28 targets in S/G2/M phases to Swi4 levels, we took advantage of the fact that Cdc28 is activated by Cln3 in early G1 phase. A *CLN3* deletion decreased the rate of accumulation of Swi4-GFP as a function of cell size by ~46%, similar to the decrease observed upon mutating all MCB and SCB sites (Fig. 2D, Table 1). The large size phenotype of the *CDC28-as1* and *cln3Δ* strains was apparent in the large average cell sizes observed for cells exhibiting nuclear Swi4-GFP in our images (Fig S1, Table 1) and in Coulter counter measurements (Fig. S3F, Tables 1, S3). Taken together, these results demonstrate that Swi4 amplification in G1 requires Cln3-Cdc28 kinase activity.

Due to the functional overlap between SBF and MBF, and the shared ability of Swi4 and Mbp1 to bind the same SCB/MCB sites (4, 5, 22, 25), it is in principle possible that MBF could contribute to Swi4 expression. However, the lack of any effect of *MBP1* deletion on the rate of Swi4 copy number accumulation versus cell size (Table 1, Fig. 2E), suggested Mbp1 does not mediate Swi4 production. Swi4 accumulation in a strain deleted for the repressor of SBF, Whi5, led to non-linear accumulation with respect to size (Fig. 2F). Newborn daughter *whi5Δ* cells are very small, 5 fL, and have only ~14 copies of Swi4 (~7 dimers), which is extremely sub-stoichiometric with respect to the ~200 G1/S promoters. In this strain, the size dependence of Swi4 copy number was best described with an exponential function (Table 1). We note that the cell-to-cell variation in Swi4 concentration for all strains examined is much larger than the variation in Swi4 protein copy number (Fig. S5). Since copy number is computed as the nuclear Swi4 concentration multiplied by the nuclear volume, this means that the stochasticity is mostly associated with the growth rates of individual cells, and not the Swi4 accumulation rate, which is more robust. This observation suggests that Swi4 accumulation and cell growth can be independently modulated.

Ectopic Swi4 protein expression increases endogenous Swi4 protein levels

A prediction of Swi4-dependent *SWI4* expression is that an acute ectopic increase of Swi4 in G1 cells should stimulate endogenous *SWI4* transcription and an increase in endogenous Swi4 protein. We therefore examined the effect of ectopic expression of unlabeled Swi4 on the

production of Swi4-GFP from the endogenous promoter. We constructed a strain that constitutively expresses a chimeric *Z3EV* transcription factor from the ACT1 promoter with an additional copy of the *SWI4* gene under the control of a *Z3EV* -responsive promoter at the BUD9 locus (26–28). The *Z3EV* transcription factor is composed of the human Znf268 zinc-finger DNA binding domain, which recognizes a 9 base pair sequence, fused to the ligand binding domain of the estrogen receptor, which is responsive to β-estradiol (BE2). Hence, the activity of this chimeric TF, and therefore the transcription of the exogenous SWI4 gene cassette, is BE2-dependent. In a control strain to assess BE2-dependent expression, Swi4-GFP was expressed from the *Z3EV* promoter, while the endogenous copy of *SWI4* remained unlabeled (*Z3EV-SWI4-GFP*). We used this strain to measure how much Swi4 protein was produced by the *Z3EV* promoter as a function of BE2 concentration. BE2-dependent expression and nuclear localization of Swi4-GFP was observed as expected, with intensities of Swi4-GFP at a background level in absence of BE2 (Fig. 3E, Fig. S6) and reaching saturation in presence of 5 nM BE2. We note that strong and prolonged overexpression of Swi4-GFP in this strain upon addition of saturating 5 nM BE2 (Fig. 3B) led to cytokinesis defects (Fig. S6D).

In an experimental strain, the exogenous Swi4 expressed from the *Z3EV* promoter copy was unlabeled, while Swi4-GFP was expressed from the endogenous *SWI4* promoter (*Z3EV-SWI4, swi4::SWI4-GFP*). We used this strain to measure how much Swi4 protein was produced by the endogenous promoter in response to ectopic Swi4 induction as a function of BE2 concentration (Fig. 3A-D, E-blue). We observed a substantial increase in the endogenous Swi4-GFP expression with increasing concentrations of BE2. This result confirmed a key prediction, i.e., that additional ectopic Swi4 should increase endogenous Swi4-GFP expression.

As over-expression of Swi4-GFP led to a cytokinesis defect in asynchronous populations, homeostatic cell size at the population level could not be used as a readout for acceleration of Start in response to BE2 in the *Z3EV* strains. To directly examine the effect of Swi4 over-expression on the timing of Start we collected small G1 daughter cells from the *Z3EV-SWI4,swi4::SWI4-GFP* strain synchronized by centrifugal elutriation. We then measured the time-dependence of Swi4-GFP production in absence of BE2 and in presence of 5 nM BE2 using imaging conditions that minimize photo-bleaching (17). In presence of 5 nM BE2, the endogenous Swi4-GFP intensity increased markedly as a function of time, whereas in the absence of BE2 the signal was comparable to that observed in the WT strain expressing Swi4-GFP (Fig. 4A, B).

Increasing Swi4 levels accelerates the timing of Start

We have previously shown that Swi6 copy number in G1 phase is in excess compared to Swi4 and, moreover, that the Whi5/Swi4 ratio in WT cells grown in glucose medium depends on cell size, decreasing from ~2.4 in small cells to ~1.2 in large G1 cells (6). We thus expected that increased Swi4 production in response to BE2 would increase the number of active SBF complexes to levels sufficient to overcome Whi5 inhibition, leading to an acceleration of Start. In time course imaging experiments, we found that the budding index (i.e., fraction of cells in the FOV exhibiting buds) increased more rapidly in presence of 5 nM BE2 than in its absence for the *Z3EV-SWI4 swi4::SWI4-GFP* strain (Fig. 4C).

Premature budding should also correlate with an increased expression of the G1/S regulon as ectopic Swi4 accumulates. To test this hypothesis, we performed a whole-genome RNA-sequencing time-course following treatment of a *Z3EV-SWI4* strain in absence and presence of 5 nM BE2. BE2-dependent expression of *SWI4* led to an increase in expression of several key G1/S regulon genes, including *CLN1* and *PCL1* (Fig. 5A,B, Table S3A). A number of SBF and MBF target genes were also down-regulated in a time dependent manner after BE2 , including a known

MBF target, Cdc21 (Fig. 5C,D, Table S3B). These results demonstrate that ectopic production of Swi4 is sufficient to prematurely activate G1/S transcription and Start.

A threshold of Swi4 protein copy number gates Start across environmental and genetic conditions

The above results reveal that genetic contexts that affect the critical cell size at Start also modulate the rate of Swi4 accumulation with respect to growth rate, suggesting the existence of a potential threshold in Swi4 copy number required for Start. We used our prior determination of the cell size at Start, 28 fL, for WT cells grown in glucose (6) to compute how many Swi4 molecules must be present in the cells when they pass Start. Under the above growth conditions, the doubling time for WT cells was 105 ± 4 (Table S2). WT cells spend about 40% of the cell cycle in G1 phase (29), which under our growth conditions corresponds to ~42 minutes, during which time they grow from ~10 to ~28 fL. This corresponds to a growth rate in G1 phase of 0.42 fL/min (=18 fL/42 min). With a birth volume of ~10 fL, where ~45-50 Swi4 molecules are present (average values over the 5 smallest cells), and a measured accumulation rate with respect to cell size of 7.9 molecules/fL (Table 2), we calculated a threshold of ~190 Swi4 molecules present at Start when the cells reach ~28 fL (, i.e., 45-50 molecules at birth + 18 fL growth in G1*7.9 molecules/fL).

We next tested whether a unique threshold of 190 Swi4 molecules could explain the cell size at Start for the other strains described above. First, we estimated cell size and Swi4 copy number at birth as the average experimental values for size and copy number present in the five smallest cells detected for a given strain or condition (Fig. 2). We then used the observed accumulation rate with respect to cell size to compute how much growth occurs prior to reaching the predicted 190 molecule threshold. Specifically, we calculated the Swi4 accumulation rate versus time (copy number/min) as the product of the measured Swi4 accumulation rate versus size (copy number/fL, Table 1) and the growth rate in G1 phase (fL/min). Since doubling times for the different strains tested here were the same as for WT (Table S2), we assumed the same growth rate in G1 phase and the same fraction of the cell cycle in G1 phase as for WT. Note that if we assume a larger fraction of the cell cycle in G1 phase (equivalent to a proportionally faster growth rate for the same fraction) then predicted size at Start is slightly larger (Table 2). For diploid cells, using the reported 33% faster diploid growth rate compared to haploids (30), the average growth rate was calculated proportionally to be 0.73 fL/min. For all of these strains, except *whi5Δ* cell size at Start corresponds to the size at which the threshold of 190 Swi4 copies is reached (Fig. 6A).

This simple Swi4 threshold hypothesis provides reasonable predictions of cell size at Start for most of the strains examined here, with the exception of *whi5Δ* (Table 2, Fig. 6B). An increased size at Start is predicted for the strains with deficient phosphorylation (*CDC28as1* + drug and *cln3Δ*) (24, 31). The threshold hypothesis also predicts a larger cell size for the promoter mutant strains, although the predicted sizes are somewhat larger than those derived from Coulter Counter measurements. Most dramatically, size at Start for WT diploid cells is predicted to be ~80% larger than that of haploids (Table 2). A threshold of 190 Swi4 copies is also consistent with the small size of cells grown in glycerol (32–34). We observed previously that compared to glucose medium, cells of the same size grown in glycerol medium had ~20% more Swi4 copies (6). This positive differential scaling of Swi4 accumulation vs growth in poor nutrients results in cells reaching the Swi4 threshold at a smaller size than when grown in glucose (Fig. 6A, red). Assuming a growth rate in glycerol medium of 0.3 fL/min, calculated from the ratio of doubling times in the two media and a 67% increase in the fraction the of cell cycle in G1 phase in glycerol medium (6), yields a predicted size at Start in glycerol medium of 22.2 fL (Table 2). The

threshold value which results in a correct prediction of size at Start for *whi5Δ*, 110 Swi4 copies, is much lower than the 190 copies that correctly predicts size for the other strains.

Discussion

The role of Swi4-dependent *SWI4* transcription in the Start transition is supported by four main lines of evidence: (i) quantitative sN&B measurements that show that the rate of accumulation of Swi4 depends on the presence of Swi4 target sites in the *SWI4* promoter; (ii) dependence of Swi4 accumulation rate on Cln3-Cdc28 activity; (iii) ectopic Swi4-mediated induction of endogenous Swi4 expression and acceleration of G1/S transcription; (iv) decreased rate of Swi4 accumulation in diploids with respect to growth and concomitantly larger cell size. Swi4-dependent *SWI4* transcription is responsible for approximately half of Swi4 accumulation in G1 phase in haploid cells grown in glucose medium. Interestingly, the contribution of Swi4 autoregulation to Swi4 accumulation corresponds to the difference in accumulation rate of Swi4 with respect to that of the other G1/S TFs (Swi6, Whi5, and Mbp1), all of which scale approximately linearly with growth, i.e., constant concentration with size (6). The interconnected feedback loops of Swi4 production, Cln1/2 production (14) and SBF/Whi5 phosphorylation (8, 9, 35) all likely contribute to a sharp and effectively irreversible Start transition.

Our measurements suggest that a threshold of 190 Swi4 monomers may titrate the ~200 promoters in the G1/S regulon to activate Start. This titration model predicts cell size reasonably well for the strains and conditions examined except *whi5Δ*. In addition to the haploid mutant strains, the Swi4 threshold of 190 Swi4 monomers per haploid genome correctly predicts the near doubling of cell size for diploids, due to the decreased rate of Swi4 accumulation when normalized to the diploid genome. The threshold also predicts the small size at Start of WT cells grown in poor nutrients. In this case growth is slowed more than the accumulation of Swi4 such that cells reach the Swi4 threshold at a smaller size. This SBF promoter titration hypothesis is reminiscent of a previous titration model in which G1/S promoters are titrated by Cln3 (37).

Reasonable predictions based on the threshold for the *cln3Δ* and *CDC28-as1* strains demonstrate that the Swi4 copy number threshold per se is not dependent on phosphorylation, while the rate of Swi4 accumulation is. In absence of Whi5 repression, the inherent positive feedback in Swi4-dependent Swi4 production is unmasked. More Swi4 molecules lead to more active SBF and an increase in the rate of Swi4 accumulation with size, *i.e.*, an exponential increase of Swi4 copy number. Moreover, the *whi5Δ* cells pass Start at a smaller size (7), and with a lower Swi4 copy number than WT cells, perhaps because all SBF complexes are de-repressed and contribute to transcription. The empirical threshold of 190 Swi4 molecules would represent some threshold of active SBF complexes. In absence of Whi5, the number of active SBF per Swi4 copy number is higher, thus requiring fewer Swi4 copies to reach the level of G1/S regulon activation required for Start.

In small cells, SBF and MBF dimers are strongly limiting with respect to the ~200 promoter targets in the G1/S regulon (6). This is especially true for Swi4(SBF) which is present at very low copy number in newborn cells. The increase in SBF copy numbers during G1 phase leads to a corresponding increase in G1/S promoter occupancy by inactive Whi5-SBF complexes. We speculate that transient equilibrium dissociation of Whi5 may allow the stochastic expression of *SWI4*, *CLN1* and *CLN2* (and likely other G1/S regulon genes), but that the stability of the Swi4 protein allows its gradual accumulation compared to the unstable cyclins. The exponential accumulation of Swi4 in a *whi5Δ* strain is consistent with this idea. While ~190 Swi4 monomers corresponds to only 95 Swi4 dimers (6), about half the total target promoters in the G1/S regulon, once activated by phosphorylation, this pool might be sufficient to activate the whole G1/S regulon. Notably, clustering of SBF complexes and presumably target G1/S genes, may enable a limited pool of SBF complexes to activate the entire G1/S regulon (38).

The molecular mechanisms responsible for the differential scaling of Swi4 accumulation with respect to growth observed here remain to be determined. For example, why does the Swi4 accumulation rate slow less than bulk growth rate in poor nutrients? And similarly, while the observed lower Swi4 accumulation rate in diploids may help account for the size relationships of ploidy, the mechanism for this reduced accumulation rate (per haploid genome) in diploids remains to be discovered. Different environmental conditions may also alter the threshold number of Swi4 molecules required for Start. Rapid and irreversible switch transitions are implicated in many important cellular processes such as development, differentiation and damage responses. Transcription factor autoregulation and titration of target promoters in complex regulons may be a recurrent regulatory motif in many of these transitions.

Materials and Methods

Experimental Design

The objective of the study was to quantify the accumulation of the Swi4 transcription factor with respect to cell size and to test the effects of genetic backgrounds relevant to the control of the G1/S transition. The Swi4 protein, expressed form its natural locus as a GFP fusion in these strains was quantified by the scanning Number and Brightness particle counting approach as implemented in (6). Budding yeast strains used in this work are summarized in Table 3.

Yeast Strain Construction

All haploid experimental strains were generated in BY4741 derivative of S288C background strain with PCR-based homologous recombination integration of a *mGFPmut3-HIS3MX* cassette at the C terminus of the Swi4 natural locus, which were crossed into other BY4741 mutant strains as needed. A strain producing monomeric GFP from an inducible promoter that would be used in molecular brightness calculations was obtained by transforming <*pGAL1-mGFPmut3 CEN URA3*> plasmid into BY4741 strain. None of the experimental strains exhibited noticeable cell size and growth phenotype difference from their untagged wild type counterparts.

The β-Estradiol (BE2) inducible strains were constructed by using *Z3EV* expression strain DBy19004 (MTy5193) (38) together with the transformation of *mGFPmut3-HIS3MX* cassette at Swi4's natural locus, *ura3Δ::NatMX, bud9Δ::ACT1pr-Z3EV-ENO2term-URA3-Z3EVpr(P1)-GFP-Gal80term* as background strain. In this strain, the *Z3EV* artificial transcription factor with *ACT1* promoter and *ENO2* terminator was integrated to replace bud9 to express *Z3EV*, the gene under the *Z3EV*-responsive promoter *Z3EVpr(P1)*, which contains binding sites for *Z3EV*, express conditionally upon β-estradiol addition to the culture. We built a key strain *Z3EV-SWI4* with *swi4::SWI4-GFPmut3* (MTy5189) for *SWI4*-dependent *SWI4* induction. Firstly, PCR fragment based homologous recombination integrated *SWI4-hphMX* under *Z3EV* promoter (P1) to replace GFP in strain DBy19004 to build *Z3EV-SWI4* strain MTy5188. Then homologous recombination integrated fragment *mGFPmuts3-KanMX* to the C-terminus of endogenous *SWI4* locus to obtain *Z3EV-SWI4, swi4::SWI4-mGFP* strain (MTy5189). We also built a control strain *Z3EV-SWI4-mGFP* to ensure that Swi4-mGFP is expressed and measured under the level of BE2 induction. Using DBy19004 as background strain, we integrated *SWI4-mGFP-HisMX* under the *Z3EVpr(P1)* promoter by homologous recombination to replace the original GFP in DBy19004 to yield *Z3EV-SWI4-mGFP,SWI4WT* strain (MTy5190).

Cell Culture and Growth in Liquid Medium

All experimental strains were grown in Synthetic Complete (SC) medium with 2.0 g/L amino acid (Sunrise Science)) mix supplemented with 6.7 g/L yeast nitrogen base (Sigma-Aldrich) and 2% w/v glucose. For each SN&B experiment, a single colony of appropriate background strain, free GFP strain and the GFP-tagged strains of interest were grown in 1 mL SC 2% glucose medium to saturation overnight. The saturated overnight cultures were diluted 1/30 in 1 ml SC 2% glucose medium and grown to early exponential phase (4-5 hours) before imaging.

For synchronous time course experiments in presence of BE2, early G1 cells obtained by centrifugal elutriation were induced with 5 nM or 0 nM BE2 + SC 2% glucose media for 15 minutes at 300C, and added to SC glucose agarose pads containing 5 nM or 0 nM BE2 prior to imaging. The strain expressing the analog sensitive allele of the Cdc28 kinase was induced with 10 mM ATP analog drug; 1- (tert-butyl)-3-(naphthalen-1-ylmethyl)-1H-pyrazolo [3,4-d] pyrimidin-4-amine, referred to as 1- NM-PP-1, directly on agarose pads. Cells were grown on these pads for 20 minutes prior to imaging. For GFP induction of the *GAL1-GFPmut3* strain used for GFP brightness calibration, after overnight growth to saturation in SC glucose medium, the culture was washed, diluted 1/30 and grown in SC 2% raffinose medium for 3-4 hours. This was followed by the addition of 0.1% galactose to the culture for 1 hour. The induced culture was then washed twice with SC 2% glucose medium and grown in SC 2% glucose medium for 3-4 hours before imaging to approximate similar growth and culture conditions as the control and protein fusion strains.

Mounting of Cells on Agarose Pads

Before each SN&B experiment, 200 µL from a 1 ml culture grown to early exponential phase (OD600 of 0.16-0.18, cell density 1-2 x 106 cells/mL) was pelleted in a microfuge at 1300 RPM for 30 seconds and 195 µL of the supernatant was discarded. Cells were immediately re-suspended in the remaining 5 µL medium, and 3.5 µL of the suspension was mounted onto a 2% glucose agarose pad (62µL) as previously described (Dorsey et al, 2018). The agarose pad containing mounted cells was sealed with a ConA (Sigma, 2 mg/mL)-coated coverslip for immobilization of cells during imaging. The sealed pads were clamped in an Attofluor chamber (Molecular Probes) and clusters of monolayer cells were imaged for no longer than 2 hours.

Elutriation of BE2 dependent strains

Centrifugal elutriation was used to extract synchronous G1 cells for the time-course imaging on WT *SWI4* (MTY 5270) and *Z3EV* strain (MTY 5189). Cells were cultured in 1.2 l of SC + 2% glucose overnight to early exponential growth phase (0D600=0.14 measured using a Tecan Infinite M1000 Pro Plate Reader), and centrifuged in a Sorvall SLC-6000 rotor at 1100 rpm for 10 min at 4°C. Using 50ml of the supernatant as the sample medium, cells were collected, softly sonicated (30 s, 1 s intervals at power level 1), and eluted at 1500 rpm in a Beckman JE-5.0 centrifugal elutriator. 8 ml/min of cells were put into the elutriator, and 12 ml/min of elution were collected. The 50 ml of eluted cells was pelleted in a microfuge at 1300 RPM for 30 seconds and 195 µL of the supernatant was discarded. Cells were immediately re-suspended in the remaining 5 µL medium. WT *SWI4-GFP* (MTY 5270) was likewise rested in the re-suspended medium for 15 minutes before mounting on pad for imaging. Finally, 3.5 µL of the suspension was mounted onto a 2% glucose agarose pad (62µL) as previously described (6).

Scanning Number and Brightness (SN&B) Imaging

For accurate quantitative measurement of absolute concentrations of Swi4, we used an image based variation of particle-counting fluctuation microscopy technique called SN&B (39). The sN&B acquisitions were performed in an ISS Alba fast scanning mirror fluctuation microscope (ISS, Champaign, IL) equipped with 2-photon laser excitation (Mai Tai Ti: Sapphire, Newport-SpectraPhysics, Mountain View, CA) at an excitation wavelength of 1000 nm. Emission from GFP was obtained using a 530 +/- 50 nm band-pass filter. Acquisition for each strain was done in multiple FOVs with the FOV size of 256x256 pixels covering 20x20 mm. Each FOV was scanned with 50 raster scans at a 40 us pixel dwell-time. Further, each FOV was imaged in 3 z-positions separated by 500 nm.

Steady-state and time course imaging of BE2 dependent strains

In steady-state BE2 experiments, the WT *SWI4-GFP* strain (MTy 5270) and the experimental and control *Z3EV* strains, MTy5189 and MTy5190, respectively, were imaged as for all other strains except that in addition cells were incubated for 30 minutes in SC medium containing 0-5 nM concentrations of BE2 after reaching the early exponential phase of growth.

The BE2-induced cultures were centrifuged, the supernatant washed off, and induced cells were grown in 1ml SC 2% glucose media for 1 hour before mounting on agarose pads for imaging.

In the BE2 time courses, early G1 cells of WT *SWI4-GFP* (MTy 5270) and the BE2 strains (MTy 5189 and MTy5190) obtained through centrifugal elutriation were treated with 5 nM BE2 for 15 minutes and mounted onto a 2% glucose agarose pad as described above. WT *SWI4-GFP* was imaged using ISS Alba fast scanning mirror fluctuation microscope (ISS, Champaign, IL) equipped with 2-photon laser excitation (Mai Tai Ti: Sapphire, Newport-SpectraPhysics, Mountain View, CA) at an excitation wavelength of 1000 nm at 31% power. Emission from GFP was collected using a 530 +/- 50 nm band-pass filter. To avoid photobleaching, a new FOV was imaged every time point for 10 scans at 40 µs pixel dwell time at 3 z-positions separated by 500 nm. BE2 Strain was imaged using ISS Alba fast scanning mirror fluctuation microscope (ISS, Champaign, IL) using excitation of a 488nm wavelength laser (Becker and Hickl GmbH, Berlin, Germany) of 20MHz pulse frequency with its power calibrated to comparable excitation of GFP as with 1000nm 2p laser at 30% intensity. To avoid photobleaching by 1-photon excitation, a new FOV was imaged every time point for 25 scans at 40 µs pixel dwell time at one z-position.

Coulter Counter Cell Sizing and Growth Curve

The size phenotypes of all strains were acquired using a Beckman Coulter Counter Z2 particle sizer calibrated to a default 31.02 diameter calibration constant. For sizing the cells, saturated overnight cultures were diluted 1/30th in 1 ml SC 2% glucose medium and grown to early exponential phase (4-5 hours). 200 µL of culture was added to 10 ml of Beckman Isoton II diluent solution and sonicated lightly for 30 seconds before size acquisition. The number of cells per binned cell sizes were divided by total particle count to analyze for percentage fraction of cells by number vs cell size.

For assessing the growth rate of different strains, used cells were grown in 1 ml overnight culture as described above. The saturated culture was diluted 1/30th in 1ml SC 2% glucose medium. Following the dilution, the 200 µL of the growing cultures were taken every hour and added onto a Grenier 96-well flat transparent plate and their absorbance was measured at 600 nm (OD600). Immediately following the acquisition, 200 µL of culture was pipetted back to the 1 ml growing culture for absorbance reading every hour until saturation.

Scanning Number and Brightness Image Analysis

Our methodology for sN&B analysis has been described previously (Dorsey et al., 2018), but we will briefly summarize it here. For absolute quantification of fluorescent proteins using SN&B, we employ a method for probabilistic auto-fluorescent background subtraction, based on comparing the distribution of background intensities from hundreds of millions of pixels of images from cells that do not express FP fusions to a probabilistic calculation of the background intensity at every pixel in the FOV from cells expressing specific fluorescent protein fusions. Two calibration parameters were performed for obtaining the absolute concentrations of GFP-tagged proteins. First, the effective volume of the microscope, V_{PSF}, defined by laser alignment, was obtained for each experiment by sN&B using a solution of 46 or 28 nM fluorescein in Tris buffer (pH 8.0) and 40% glycerol. Second, an *in cellulo* sN&B calibration of the molecular brightness of free monomeric GFP, e_{GFP}, was performed using cells expressing monomeric GFP from a plasmid (6) to compute the concentrations of the GFP fusion proteins. For the *SWI4-GFP* strains examined, the absolute concentration of nuclear Swi4-GFP in each cell was calculated from the average intensity of all nuclear pixels after background subtraction, $\langle F \rangle_{nuc}$, as:

$$[Swi4]_{nuc}\,(M) = \langle F \rangle_{nuc} / (e_{GFP} * V_{PSF} * N_A) \qquad [1].$$

Nuclear volume for individual cells was calculated as 1/7 of the total cell size (23) derived from whole cell masking and assuming a sphere.

All sN&B acquisitions were analyzed using custom 2015 MATLAB scripts (Sylvain Tollis, University of Montreal with edits from Steven Notley and Catherine Royer, RPI), which has previously been used to determine absolute concentration of fluorescent proteins in live cells (6, 40). This semi-automated analysis allowed the computation of absolute protein concentrations in the best Z-position for select regions of interest i.e., the nucleus of pre-start cells. Standard deviations of the *dSwi4/dsize* plots (Fig. 2) were derived from the residuals of the linear fits.

BE2 Intensity Analysis

All analysis of fluorescence intensity of Z3EV strains were performed in the analysis software SimFCS (Enrico Gratton, Laboratory of Fluorescence Dynamics, UC Irvine). Fluorescence intensity from 5 FOVs at each BE2 concentration were averaged and plotted in Figure 4. All fluorescence intensity images were using SimFCS at 0-14 intensity units for all images.

RNA-seq analysis

The Z3EV-SWI4-hphMX cells were grown as described above for sN&B experiments and induced for 1 h with either 5 nM of BE2 (in ethanol solvent) or ethanol as a negative control. Total RNA was prepared as described in (41) both before (pre-induction sample) and after induction. Briefly, cells were disrupted using glass beads, and their aqueous content was extracted using phenol/chloroform. Nucleic acids were then precipitated using ethanol and genomic DNA was removed using DNase treatment (Qiagen). RNA was quantified using Qubit (Thermo Scientific) and assessed for quality with a 2100 Bioanalyzer (Agilent Technologies). Poly-A selected transcriptome libraries were generated using the Kapa RNA HyperPrep (Roche). Sequencing was performed on the Illumina NextSeq 500 system. Experiments were performed in duplicate.

RNA-sequencing data analysis was performed as detailed in (40). Briefly, raw reads were aligned to all Ensembl yeast transcripts using Bowtie 2.2.5 (42) with default parameters and counts were defined as alignments with an edit distance smaller than 5. Dubious ORFs as annotated in the Saccharomyces Genome Database were excluded. Only genes with at least 500 reads in one samples were further analyzed. Gene expression levels were expressed as log2 read counts, normalized to the upper-quartile gene expression level for each sample separately (43). For each of the two replicates, the expression after 1 h BE2 induction was normalized separately to the expression in the pre-induction sample and in the control ethanol-treated sample of the same replicate, yielding four fold-change values for each gene. Then, the smallest of those log2 fold-change (in absolute value) was used to generate the final differential expression profile represented on Figure 5. Hence, a gene had to be upregulated (or respectively downregulated) with respect to both the pre-induction and the ethanol-treated sample across both replicates to get a positive (resp. negative) score, the former control reducing sample-to-sample variation while the second eliminates BE2-independent but time-dependent gene expression variation in the cell population. Genes for which any of the four normalizations yielded log2 fold changes of different signs were assigned a score of 0. Among the most up- and down-regulated genes, direct SBF and/or MBF targets were identified based on Ferrezuelo et al. (44). At each ranking position n, the enrichment of SBF targets (for upregulated genes) or MBF targets (for downregulated genes) within the nth top differentially regulated genes as compared to random expectations was computed, and the significance of the enrichment level was calculated using Fisher's exact test.

References

1. C. Bertoli, J. M. Skotheim, R. A. M. De Bruin, Control of cell cycle transcription during G1 and S phases. Nat. Rev. Mol. Cell Biol. 14, 518–528 (2013).
2. J. DeGregori, T. Kowalik, J. R. Nevins, Cellular Targets for Activation by the E2F1 Transcription Factor Include DNA Synthesis- and G 1 /S-Regulatory Genes. Mol. Cell. Biol. 15, 4215–4224 (1995).
3. C. Koch, T. Moll, M. Neuberg, H. Ahorn, K. Nasmyth, A role for the transcription factors Mbp1 and Swi4 in progression from G1 to S phase. Science 261, 1551–7 (1993).
4. V. R. Iyer, C. E. Horak, C. S. Scafe, D. Botstein, M. Snyder, P. O. Brown, Genomic binding sites of the yeast cell-cycle transcription factors SBF and MBF. Nature 409, 533–538 (2001).
5. J. M. Bean, E. D. Siggia, F. R. Cross, High functional overlap between MluI cell-cycle box binding factor and Swi4/6 cell-cycle box binding factor in the G1/S transcriptional program in Saccharomyces cerevisiae. Genetics 171, 49–61 (2005).
6. S. Dorsey, S. Tollis, J. Cheng, L. Black, S. Notley, M. Tyers, C. A. Royer, G1/S Transcription Factor Copy Number Is a Growth-Dependent Determinant of Cell Cycle Commitment in Yeast. Cell Syst. 6, 539-554.e11 (2018).
7. P. Jorgensen, J. L. Nishikawa, B.-J. Breitkreutz, M. Tyers, Systematic identification of pathways that couple cell growth and division in yeast. Science. 297, 395–400 (2002).
8. R. A. M. de Bruin, W. H. McDonald, T. I. Kalashnikova, J. Yates, C. Wittenberg, Cln3 activates G1-specific transcription via phosphorylation of the SBF bound repressor Whi5. Cell 117, 887–898 (2004).
9. M. Costanzo, J. L. Nishikawa, X. Tang, J. S. Millman, O. Schub, K. Breitkreuz, D. Dewar, I. Rupes, B. Andrews, M. Tyers, CDK activity antagonizes Whi5, an inhibitor of G1/S transcription in yeast. Cell 117, 899–913 (2004).
10. L. Breeden, Start Specific Transcription in Yeast (1996)vol. 208.
11. H. E. Richardson, C. Wittenberg, F. Cross, S. I. Reed, An essential G1 function for cyclin-like proteins in yeast. Cell 59, 1127–1133 (1989).
12. G. E. Neurohr, R. L. Terry, J. Lengefeld, M. Bonney, G. P. Brittingham, F. Moretto, T. P. Miettinen, L. P. Vaites, L. M. Soares, J. A. Paulo, J. W. Harper, S. Buratowski, S. Manalis, F. J. van Werven, L. J. Holt, A. Amon, Excessive Cell Growth Causes Cytoplasm Dilution And Contributes to Senescence. Cell 176, 1083-1097.e18 (2019).
13. M. Tyers, G. Tokiwa, B. Futcher, Comparison of the Saccharomyces cerevisiae G1 cyclins: Cln3 may be an upstream activator of Cln1, Cln2 and other cyclins. EMBO J. 12, 1955–68 (1993).
14. J. M. Skotheim, S. Di Talia, E. D. Siggia, F. R. Cross, Positive feedback of G1 cyclins ensures coherent cell cycle entry. Nature 454, 291–6 (2008).
15. K. M. Schmoller, J. J. Turner, M. Kõivomägi, J. M. Skotheim, Dilution of the cell cycle inhibitor Whi5 controls budding-yeast cell size. Nature 526, 268–72 (2015).
16. K. M. Schmoller, M. C. Lanz, J. Kim, M. Koivomagi, Y. Qu, C. Tang, I. V. Kukhtevich, R. Schneider, F. Rudolf, D. F. Moreno, M. Aldea, R. Lucena, J. M. Skotheim, Whi5 is diluted and protein synthesis does not dramatically increase in pre-Start G1. Mol. Biol. Cell 33, lt1 (2022).

17. A. Litsios, P. Goswami, H. M. Terpstra, C. Coffin, L. A. Vuillemenot, M. Rovetta, G. Ghazal, P. Guerra, K. Buczak, M. T. ander Schmidt, Alex, S., Tyers, S. Tollis, M. Tyers, C. A. Royer, A. Milias-Argeitis, M. Heinemann, The timing of Start is determined primarily by increased synthesis of the Cln3 activator rather than dilution of the Whi5 inhibitor. Mol. Biol. Cell 33, rp2 (2022).

18. R. Foster, G. E. Mikesell, L. Breeden, Multiple SWI6-Dependent cis-Acting Elements Control SWI4 Transcription through the Cell Cycle. Mol. Cell. Biol. 13, 3792–3801 (1993).

19. C. J. McInerny, J. F. Partridge, G. E. Mikesell, D. P. Creemer, L. L. Breeden, A novel Mcm1-dependent element in the SWI4, CLN3, CDC6, and CDC47 promoters activates M/G1-specific transcription. Genes Dev. 11, 1277–1288 (1997).

20. C. J. McInerny, J. F. Partridge, G. E. Mikesell, D. P. Creemer, L. L. Breeden, A novel Mcml-dependent element CDC4S7 promoters activates M / Gi-specific transcription. 1277–1288 (1997).

21. I. Simon, J. Barnett, N. Hannett, C. T. Harbison, N. J. Rinaldi, T. L. Volkert, J. J. Wyrick, J. Zeitlinger, D. K. Gifford, T. S. Jaakkola, R. a. Young, Serial regulation of transcriptional regulators in the yeast cell cycle. Cell 106, 697–708 (2001).

22. M. R. Harris, D. Lee, S. Farmer, N. F. Lowndes, R. A. M. de Bruin, Binding Specificity of the G1/S Transcriptional Regulators in Budding Yeast. PLoS One 8, 1–8 (2013).

23. P. Jorgensen, N. P. N. P. Edgington, B. L. B. L. Schneider, I. Rupes, M. Tyers, B. Futcher, I. Rupeš, M. Tyers, B. Futcher, The Size of the Nucleus Increases as Yeast Cells Grow. Mol. Biol. Cell 18, 3523–3532 (2007).

24. A. C. Bishop, J. a Ubersax, D. T. Petsch, D. P. Matheos, N. S. Gray, J. Blethrow, E. Shimizu, J. Z. Tsien, P. G. Schultz, M. D. Rose, J. L. Wood, D. O. Morgan, K. M. Shokat, A chemical switch for inhibitor-sensitive alleles of any protein kinase. Nature 407, 395–401 (2000).

25. F. M. Bastos de Oliveira, M. R. Harris, P. Brazauskas, R. a M. de Bruin, M. B. Smolka, Linking DNA replication checkpoint to MBF cell-cycle transcription reveals a distinct class of G1/S genes. EMBO J. 31, 1798–1810 (2012).

26. Y. Arita, G. Kim, Z. Li, H. Friesen, G. Turco, R. Y. Wang, D. Climie, M. Usaj, M. Hotz, E. H. Stoops, A. Baryshnikova, C. Boone, D. Botstein, B. J. Andrews, R. S. McIsaac, A genome□scale yeast library with inducible expression of individual genes. Mol. Syst. Biol. 17 (2021).

27. M. J. Ohira, D. G. Hendrickson, R. Scott McIsaac, N. Rhind, An estradiol-inducible promoter enables fast, graduated control of gene expression in fission yeast. Yeast 34, 323–334 (2017).

28. R. S. McIsaac, B. L. Oakes, X. Wang, K. A. Dummit, D. Botstein, M. B. Noyes, Synthetic gene expression perturbation systems with rapid, tunable, single-gene specificity in yeast. Nucleic Acids Res. 41, 1–10 (2013).

29. B. J. Brewer, E. Chlebowicz-Sledziewska, W. L. Fangman, Cell cycle phases in the unequal mother/daughter cell cycles of Saccharomyces cerevisiae. Mol. Cell. Biol. 4, 2529–2531 (1984).

30. S. Di Talia, J. M. Skotheim, J. M. Bean, E. D. Siggia, F. R. Cross, The effects of molecular noise and size control on variability in the budding yeast cell cycle. Nature 448, 947–51 (2007).

31. M. Linskens, M. Tyers, B. Futcher, CLN3 Functions in Both Daughter and Mother Cells of S. cerevisiae. Cell 72, 487–489 (1993).

32. G. C. Johnston, C. W. Ehrhardt, A. Lorincz, B. L. Carter, Regulation of cell size in the yeast Saccharomyces cerevisiae. J. Bacteriol. 137, 1–5 (1979).

33. A. Lorincz, B. L. A. Carter, Control of Cell Size at Bud Initiation in Saccharomyces cerevisiae. J. Gen. Microbiol. 113, 287–295 (1979).

34. P. Jorgensen, I. Rupeš, J. R. Sharom, L. Schneper, J. R. Broach, M. Tyers, A dynamic transcriptional network communicates growth potential to ribosome synthesis and critical cell size. Genes Dev. 18, 2491–2505 (2004).

35. M. V. Wagner, M. B. Smolka, R. A. M. de Bruin, H. Zhou, C. Wittenberg, S. F. Dowdy, Whi5 regulation by site specific CDK-phosphorylation in Saccharomyces cerevisiae. PLoS One 4, e4300 1-12 (2009).

36. H. Wang, L. B. Carey, Y. Cai, H. Wijnen, B. Futcher, C. Ying, H. Wijnen, B. Futcher, Recruitment of Cln3 Cyclin to Promoters Controls Cell Cycle Entry via Histone Deacetylase and Other Targets. PLoS Biol. 7, e1000189 (2009).

37. L. Black, S. Tollis, G. Fu, J. Fiche, S. Dorsey, J. Cheng, G. Ghazal, S. Notley, B. Crevier, G1 / S transcription factors assemble in increasing numbers of discrete clusters through G1 phase. J Cell Biol 219 (2020).

38. R. S. McIsaac, P. A. Gibney, S. S. Chandran, K. R. Benjamin, D. Botstein, Synthetic biology tools for programming gene expression without nutritional perturbations in Saccharomyces cerevisiae. Nucleic Acids Res. 42, 1–8 (2014).

39. M. A. Digman, R. Dalal, A. F. Horwitz, E. Gratton, Mapping the number of molecules and brightness in the laser scanning microscope. Biophys. J. 94, 2320–32 (2008).

40. S. Tollis, J. Singh, R. Palou, Y. Thattikota, G. Ghazal, J. Coulombe-Huntington, X. Tang, S. Moore, D. Blake, E. Bonneil, C. A. Royer, P. Thibault, M. Tyers, The microprotein Nrs1 rewires the G1/S transcriptional machinery during nitrogen limitation in budding yeast. PLoS Biol. 20, 1–31 (2022).

41. G. Ghazal, J. Gagnon, P. É. Jacques, J. R. Landry, F. Robert, S. Abou Elela, Yeast RNase III Triggers Polyadenylation-Independent Transcription Termination. Mol. Cell 36, 99–109 (2009).

42. B. Langmead, S. L. Salzberg, Fast gapped-read alignment with Bowtie 2. Nat. Methods 9, 357–359 (2012).

43. J. H. Bullard, E. Purdom, K. D. Hansen, S. Dudoit, Evaluation of statistical methods for normalization and differential expression in mRNA-Seq experiments. BMC Bioinformatics 11, 1471 (2010).

44. F. Ferrezuelo, N. Colomina, B. Futcher, M. Aldea, The transcriptional network activated by Cln3 cyclin at the G1-to-S transition of the yeast cell cycle. Genome Biol. 11, R67 (2010).

Acknowledgments

The authors would like to thank Dr. Brenda Andrews for the gift of the original *Z3EV* strains.

Funding:

This work was supported by grants National Science Foundation grant PHY 1806638 (CAR) and Canadian Institutes of Health Research (FDN-167277) to M.T.

Author contributions:

Investigation: PG, AG, CC, YT
Formal analysis: PG, AG, CC, JCH
Resources. JC, GG, ST
Data curation: JCH, CAR, AG
Methodology: CAR, ST
Validation GG, JC, ST
Conceptualization: ST, MT, CAR
Software: ST, CAR,
Writing – original draft: ST, MT, CAR, AG, JC, JCH
Writing – review & editing: ST, MT, CAR
Project administration: ST, MT, CAR
Funding acquisition: ST, MT, CAR

Competing interests: Authors declare that they have no competing interests.

Data and materials availability: All data needed to evaluate the conclusions in the paper are present in the paper and/or the Supplementary Materials. Some imaging data and analysis output is available at: DOI: 10.17632/747y34j58s.1. Note that not all data are at this DOI because there is too much data to be uploaded to the database. All data will be made available upon request. The data available at the DOI will provide insight into how the experimental results were obtained.

The yeast strains can be provided by MT pending scientific review and a completed material transfer agreement. Requests for the strains should be submitted to: mike.tyers@sickkids.ca.

Figures and Tables

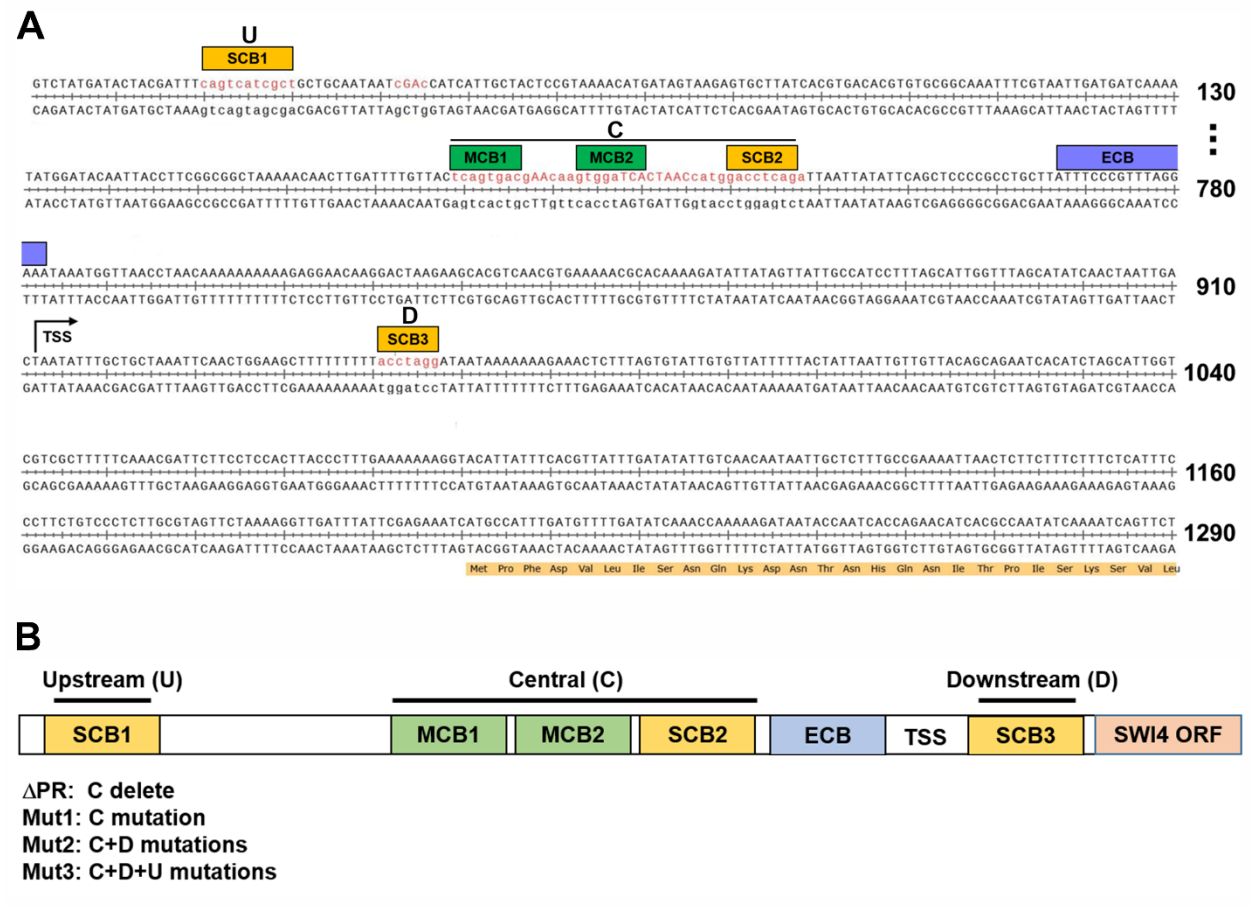

Figure 1. Mutations of the SCB/MCB sites in the SWI4 promoter. A) The region of the *SWI4* promoter containing the SCB/MCB sites deleted or mutated in this work. Green rectangles designate MCB sites, orange rectangle designates SCB site, blue rectangle designates the ECB site which was not deleted in our strains and TSS denotes the transcription start site. U refers to the upstream SCB1 site, C to the central site containing MCB1 and 2 and Scb2. D refers to the downstream SCB3 site. The beginning of the SWI4 open reading frame (ORF) is also shown. B) relative placement and nomenclature of mutated sites.

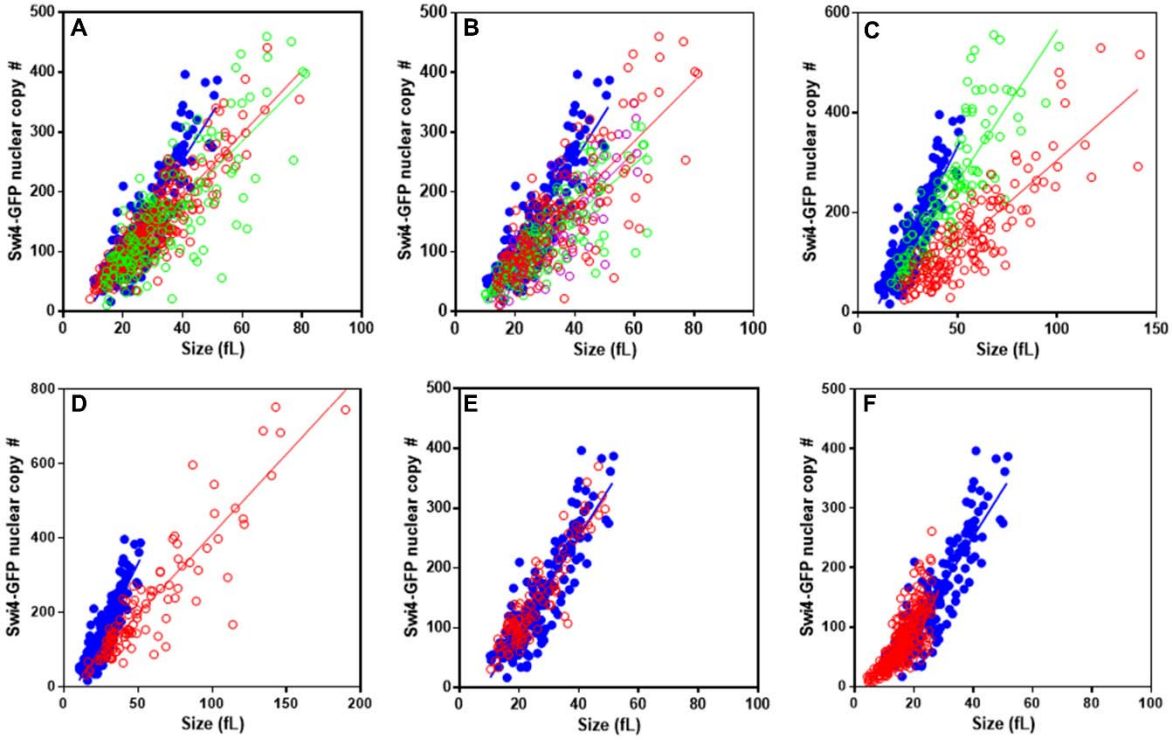

Figure 2. SCB/MCB elements in the Swi4 promoter regulate Swi4 protein production. **Figure 2. SCB/MCB elements in the Swi4 promoter regulate Swi4 protein production.** A,B) SCB/MCB sites in the SWI4 promoter contribute to the production of Swi4-GFP. Nuclear copy number of Swi4-GFP in (A) WT+*Swi4-GFP* (MTy 5314) (blue), *C delete+Swi4-GFP* (MTy 5314) (red) and *C mutations+SWI4-GFP* (MTy 5314) (green) strains; (B) WT+*Swi4-GFP* (blue), *C mutations+Swi4-GFP* (red), *C+D mutations+Swi4-GFP* (MTy 5298) (pink) and *C+D+U mutations+Swi4-GFP* (MTy5302) (green) strains; (C) WT+*Swi4-GFP* (blue), *CDC28as1+Swi4-GFP* (MTy 5317) in absence of 1-NM-PP-1 (green) and *CDC28a1+Swi4-GFP* in presence of 10 mM 1-NM-PP-1 (red); D) WT+*Swi4-GFP* (blue) and *cln3Δ+Swi4-GFP* (MTy 5318) (red) and E) WT+*Swi4-GFP* (blue) and *mbp1Δ+Swi4-GFP* (MTy 5271) (red); F) WT (blue) and *whi5Δ+Swi4-GFP* (MTy 5180) (red). Number of cells were *WT+SWI4-GFP* - 115, *C delete+SWI4-GFP* - 387, *C mutations+Swi4-GFP* - 142, C+*D mutations+Swi4-GFP* - 130, *C+D+U mutations+Swi4-GFP* - 138, *CDC28as1+Swi4-GFP* in absence of 1-NM-PP-1 - 116, and in presence of 1-NM-PP-1 - 160, *cln3Δ+Swi4-GFP* - 113, *mbp1Δ+Swi4-GFP* - 101, and *whi5Δ+Swi4-GFP* - 297.

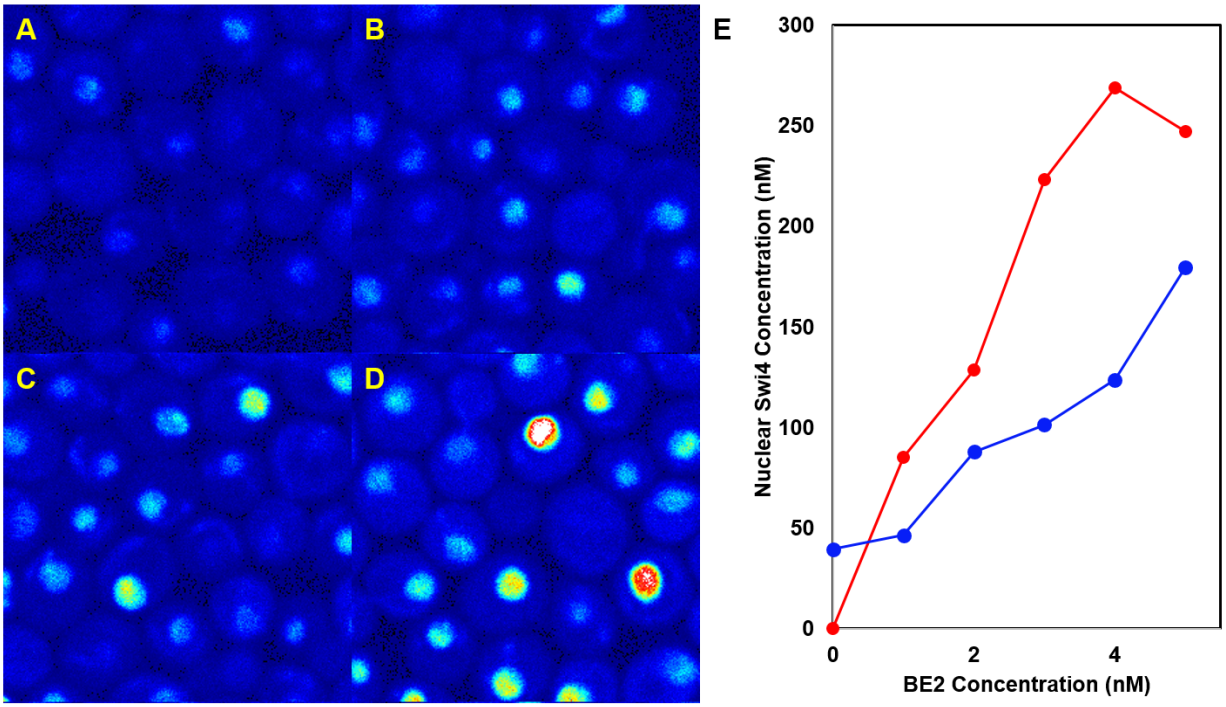

Figure 3. BE2-dependent production of Swi4-GFP. A-D) Images of FOV of the *Z3EV-SWI4*, *swi4::SWI4-GFP* strain (MTy 5189) in presence of 0, 2, 3, and 5 nM BE2, respectively. E. Swi4-GFP nuclear concentration as a function of BE2 concentration for the *Z3EV-SWI4*, *swi4::SWI4-GFP* strain (MTy5189) (blue) and the *Z3EV-SWI4-GFP-KanMX* strain (MTy 5190) (red). Image full scale is 0-8 counts. Note that in absence of BE2, the average nuclear intensity was higher in the *Z3EV-SWI4*, *swi4::SWI4-GFP* strain than for the control strain due to the presence of endogenous Swi4-GFP (6).

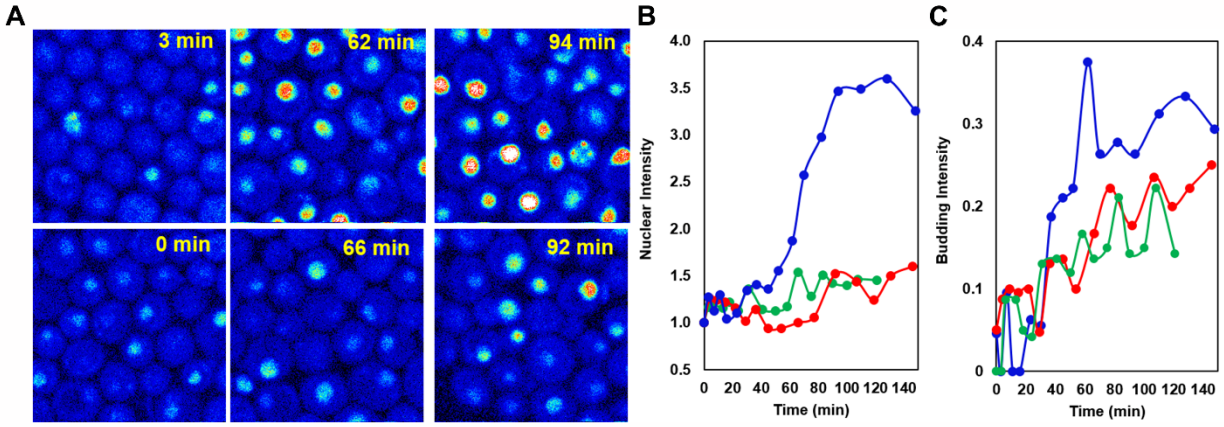

Figure 4. Time course for BE2-dependent production of Swi4-GFP. A) Images of FOV of elutriated daughter cells from the *Z3EV-SWI4, swi4::SWI4-GFP* strain (MTy5189) (top row) and the *Z3EV-SWI4-GFP-KanMX* strain (MTy5190) (bottom row) in presence of 5 nM BE2, as a function of time after addition of BE2. Time points are indicated in the images. B) Normalized intensity of nuclear Swi4-GFP as a function of time for the *Z3EV-SWI4,swi4::SWI4-GFP* strain (MTy5189) in presence of 5 nM BE2 (blue), in absence of BE2 (red) and the WT Swi4-GFP strain (green). C) Budding index as a function of time for the *Z3EV-SWI4, swi4::SWI4-mGFP* strain (MTy 5189) strain in presence of 5 nM BE2 (blue), in absence of BE2 (red) and the WT Swi4-GFP strain (MTy 5270) (green). Cells were grown in SC+2% glucose medium. Average number of cells quantified per time point was 22 ±2 for the WT Swi4-GFP time-course, 19 ±2 for the *Z3EV-SWI4, swi4::SWI4-GFP* strain in presence of 5 nM BE2 and 20 ±2 for the *Z3EV-SWI4,swi4::SWI4-mGFP* strain in absence of BE2

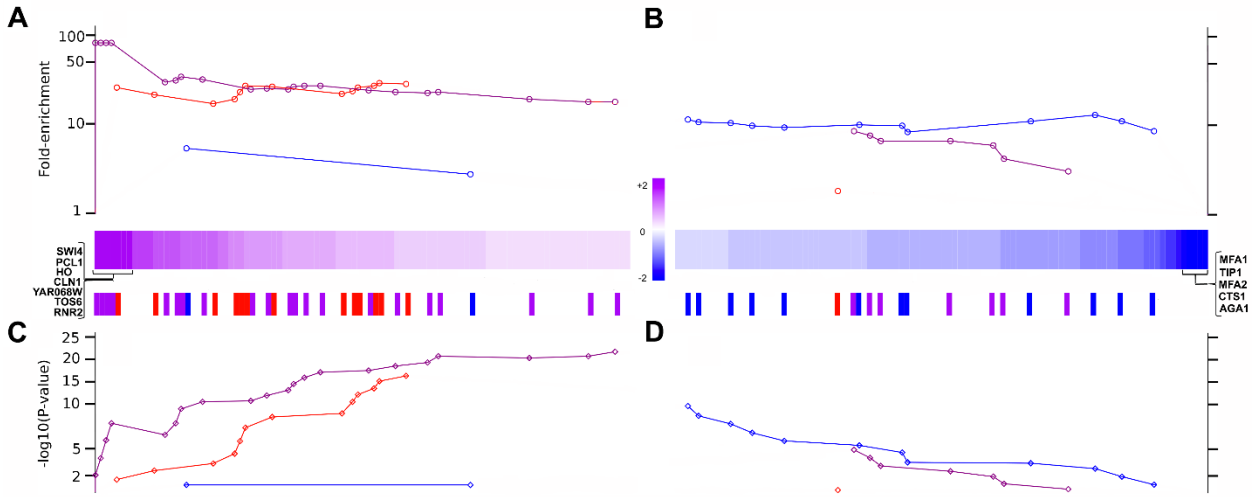

Figure 5. Effect of BE2-dependent exogenous Swi4 production on transcription of the G1/S regulon. A and B) Fold enrichment (upregulation) and fold repression (Down-regulation). In B lack of up-regulation was normalized to a fold-enrichment of 1, while the expression of the most down-regulated genes in D was normalized to 1. Colored strips represent genes that were up-regulated (pink) and downregulated (blue). The seven most strongly up-regulated genes are given on the left, while the five most strongly down-regulated genes are given on the right. Red bars below the fold enrichment strips corresponds to SBF target genes, blue bars to MBF target genes and purple-pink bars to both (41). C and D) –logP value for up-regulation (C) and down-regulation (D) compared to untreated and ethanol treated cells. Only genes with an absolute log2-fold change are shown. A complete list of the detected up- and down-regulated genes and their quantification is given in Table S2A,B.

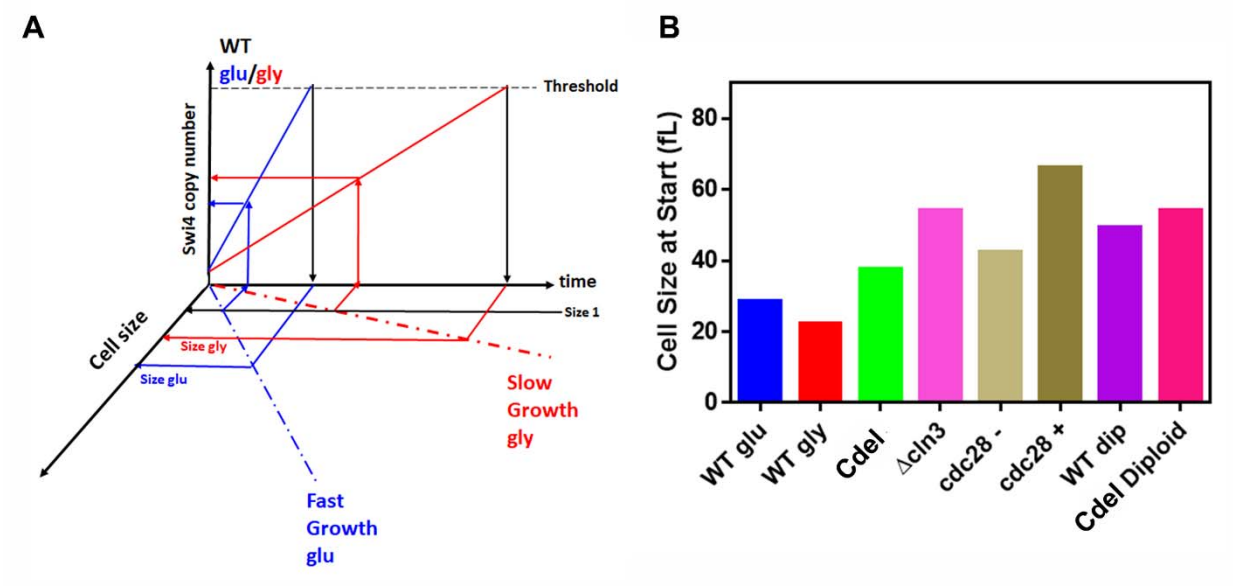

Figure 6. A unique Swi4 copy number threshold predicts cell size at Start. A) schematic of the effect of positive differential scaling between Swi4 accumulation and growth in poor nutrients (red) compared to glucose (blue). Growth is slowed by the poor nutrients more than Swi4 accumulation is slowed. Thus for cells of the same size (Size 1) there is a larger Swi4 copy number (and concentration). Since cells grow more slowly than they accumulate Swi4 in glycerol, they reach the unique threshold value required for Start at a smaller size. B) Predicted sizes at Start given the threshold hypothesis, as explained in the text and given in Table 2.

Table 1. Effect of mutations and deletions on Swi4-GFP accumulation vs cell size.

Strain	Promoter	dSwi4/size (copies/fL)	% decrease *vs* WT haploid	# cells	<size> (fL) *Cells with Nuclear Swi4
Haploid WT	WT	7.9±0.3	-	115	26.5
C delete	C deleted	5.3±0.1	33	387	29.2
C mutations	C mutated	5.0±0.3	37	142	33.6
C+D mutations	C+D mutated	4.9±0.3	38	130	30.5
C+D+U mutations	C+D+U mutated	4.3±0.3	46	138	30.1
mbp1Δ	WT	7.3±0.3	7	101	25.1
cln3Δ	WT	4.3±0.2	46	113	54.6
whi5Δ	WT	14*exp(0.09*size)		297	17.1
cdc28as - drug	WT	6.1±0.4	23	116	46.0
cdc28as + drug	WT	3.5±0.2	56	160	54.9
WT Diploid	WT	3.3±0.2	58	118	47.8
Diploid C delete	C deleted heterozygous	2.6±0.2	67	109	53.4

dSwi4/dsize is the accumulation rate of Swi4 with respect to cell size. Average size, <size>, refers to the average size of cells in the images which exhibited a nuclear Swi4-GFP signal.

Table 2. Predicted cell sizes based on the Swi4 threshold mode .

Strain	Birth vol (fL)[5]	Copy number at birth[6]	Growth rate (fL/min)[4]	Accumulation rate vs size (copy #/fL)	Size at Start (predicted,)	Size at Start (expt)
WT glucose	10	45	0.42	8	28.5	28[1]
WT glycerol	8	50	0.3	10	22.2	23.5[1]
Cdelete	10	45	0.42	5.3	37.7	30[2]
C mutation	10	45	0.42	5.0	39.4	33.0[2]
C+D mutations	10	45	0.42	4.9	39.8	33.0[2]
C+D+U mutations	10	45	0.42	4.3	44.0	34.4[2]
cln3Δ	20	45	0.42 0.70[7]	4.3	54.0 54.3[7]	59[3]
Cdc28as - drug	19	50	0.42	6.1	42.3	49[2]
Cdc28as + drug	23	40	0.42 0.70[7]	3.5	66.2 66.4[7]	-
whi5Δ	5	14		14*exp(0.09*size) threshold = 110	22.9	22.4
WT diploid	20	35	0.73	3.3	49.2	52[2]
C delete HZ Diploid	17.3	35	0.73	2.6	54.2	49[2]

Accumulation rate vs size was the slope of the plot of experimentally determined Swi4 copy number vs cell size in Figure 2 and Figure S3. [1]Experimental size at Start determined previously (Dorsey et al. 2018) for cells grown in SC+2% glucose or glycerol medium and expressing Whi5-GFP. Size at Start was determined based on cumulative frequency of all cells computed from Coulter Z2 Multi-sizer distributions and the fraction of pre-Start cells determined as those exhibiting nuclear Whi5-GFP using high resolution microscopy. Note that Whi5 exit is the earliest manifestation of Start and thus size at Start may be a slightly smaller than that determined by other means. [2]For mutant strains, the experimental size at Start was calculated as the product of WT cell size at Start in glucose medium and the ratio of median cell size of the mutant strain daughter cells with respect to WT determined by Coulter counter measurements (Table S2). [3] Reference 33. [4]Growth rate in G1 in fl/min was estimated for the WT in glucose medium as described in the text and based on Coulter counter measurements, all strains except diploid were considered to have the same growth rate in G1. Growth rate of WT in glycerol medium was estimated from the doubling time measured previously (Ref. 6) in glycerol medium (4.24 hours, compared to 2.04 hours in glucose medium in the present work) and dividing the growth rate, 0.42 fL/min, for WT by the ratio of the doubling times (4.24/2.04) corrected for the 67% larger fraction of the cell cycle in G1 phase in glycerol medium. Diploids were assumed to grow 33% faster than haploids. [5]Birth volume was that of the smallest cells observed. [6]Copy number at birth was taken as the average of the copy number for the first 5 smallest cells. [7]Cell size at Start assuming a 67% increase in the fraction of the cell cycle in G1 phase.

Table 3. Strains Used.

Strain name	MTy#	Method	Genotype
Swi4-GFP haploids			
swi4::SWI4-GFP-URA3	5270	PCR based HR mGFPmut3-URA3 marker to end of Swi4 locus in BY4741	BY4741,MATa; his3Δ 1; leu2Δ 0; met15Δ 0; ura3Δ; swi4::Swi4-mGFPmut3-ura3
swi4::SWI4-GFP-HIS	5313	Homologues recombination integrated mGFPmut3-HisMX to C-ter of SWI4 in BY4742 strain.	swi4::SWI4-mGFPmut3-HisMX-BY4742.
Haploid mutants			
whi5::NAT, SWI4::swi4-GFP-hisMX	5180	Integrated mGFPmut3-hisMX to swi4 locus in whi5::NAT (MTy2641) strain	BY4741, MATa; his3Δ 1; leu2Δ 0; met15Δ 0; ura3Δ; Whi5::NAT; Swi4::SWI4-mGFPmut3-HIS3MX
Cln3::LEU2, SWI4-GFP-HisMX	5318	genetic cross between MTy5319 (cln3::LEU2) and MTy5000 (Swi4-mGFPmut3-HisMX)	his3Δ 1; leu2Δ 0; met15Δ 0; ura3Δ; cln3::LEU2; Swi4::swi4-mGFPmut3-HisMX
mbp1::His3MX, swi4::SWI4-GFP-Ura3	5271	HIS3MX6 PCR based HR deletion of mpb1 to the MTy5270 strain Swi4::swi4-mGFPmut3-ura	BY4741,MATa; his3Δ 1; leu2Δ 0; met15Δ 0; ura3Δ; Swi4::swi4-mGFPmut3-ura3, mbp1::His3MX
cdc28::CDC28as1-NAT, swi4::SWI4-GFP3-HisMX	5317	crossed a BY4742 MATalpha cdc28-as1 strain YV264 which got from the Vogel lab (McGill University) with our MATa Swi4GFP (yMT5000). Yogitha dissected the tetrads and performed the phenotyping on selective plates	his3Δ 1; leu2Δ 0; met15Δ 0; ura3Δ; cdc28::CDC28as1-NAT; swi4::SWI4-mGFPmut3-HisMX
Haploid SWI4 promoter mutants			
SWI4prD1scbmcbswi4:Swi4-GFP-HIS3 (C delete)	5320	The central MCB and SCB sites in the Swi4 promoter are deleted. Swi4 is tagged with GFPmut3	BY4741,MATa; his3Δ 1; leu2Δ 0; met15Δ 0; ura3Δ; SWI4prD1scbmcb swi4::Swi4-GFPmut3-HIS3
swi4prSCBMCB_Mc-SWI4-GFP-HISMX (C mutations)	5314	CRISPR mutation swi4prSCBMCB site C in MTy5313. Only swi4 prSCBMCB site C mutated.	swi4prSCBMCB_Mc-SWI4-mGFP-HisMX, BY4742.
Swi4prSCBMCB_M2-SWI4-GFP-HIS3 (C+D mutations)	5298	CRISPR mutated swi4 promoter SCBMCB sites C and D, then GFP tagged mGFPmut3-HisMX to C-ter of Swi4 in BY4742	Swi4prSCBMCB_M2-SWI4-mGFPmut3-His3, By4742
SWI4prSCBMCB_M3-SWI4-GFP (C+D+U mutations)	5302	CRISPR mutated swi4 promoter upstream 1198bp SCB site U in MTy5298. All three SCBMCB sites (U, C and D) were mutated.	Swi4prSCBMCB_M3-SWI4-mGFPmut3-His3, By4742.
β-estradiol strains			
DBY19004	5193	Background strain (Mclsaac,2014)	ura3Δ::NatMX, bud9Δ::ACT1pr-Z3EV-ENO2term-URA3-Z3EVpr(P1)-GFP-Gal80term

Z3EV-SWI4-hphMX	5188	Homologous recombination replaced GFP under b/e with Swi4-hphMX in strain DBy19004 (Mclsaac,2014)	ura3Δ::NatMX, bud9Δ::ACT1pr-Z3EV-ENO2term-URA3-Z3EVpr(P1)-SWI4-hphMX-Gal80term
Z3EV-SWI4, swi4::SWI4-GFP	5189	Homologous recombination integrated mGFPmut3-KanMX to C-ter of swi4 locus in strain MTY5188 C1	swi4::SWI4-GFPmut3-KanMX, ura3Δ::NatMX, bud9Δ::ACT1pr-Z3EV-ENO2term-URA3-Z3EVpr(P1)-SWI4-hphMX-Gal80term
Z3EV-SWI4-GFP-KanMX	5190	Homologous recombination replaced GFP under b/e with Swi4-mGFPmut3-KanMX in strain DBy19004(Mclsaac,2014)	ura3Δ::NatMX, bud9Δ::ACT1pr-Z3EV-ENO2term-URA3-Z3EVpr(P1)-SWI4-GFPmut3-KanMX-Gal80term
Z3EV-Swi4, swi4::SWI4-GFP-KanMX	5273	HR integrated mGFPmut3-KanMX to C-ter of swi4 in DBy19004 strain, then replace GFP at locus under P1(b/e) with Swi4-hphMX	ura3Δ::NatMX, swi4::SWI4-GFPmut3-KanMX, bud9Δ::ACT1pr-Z3EV-ENO2term-URA3-Z3EVpr(P1)-Swi4-hphMX-Gal80term
DIPLOIDS			
Diploid, BY4742/BY4741	5309	BY4741 mate with BY4742	BY4741 X BY4742
SWI4/swi4::SWI4-GFP-HIS3 diploid	5261	swi4::SWI4-mGFP,BY4741 mate with BY4742 Diploid strain where WT Swi4 is intact in one chromosome, the other Swi4 is tagged with mGFPmut3	BY4742 X swi4::SWI4-mGFPmut2-HisMX, BY4741
SWI4/Swi4prDscbmcb swi4::SWI4-GFP-HIS3 diploid,	5263	Diploid strain where WT Swi4 is intact in one chromosome, the other Swi4 is tagged with GFPmut3 and from its promoter, the SCB MCB site C deleted	BY4741 X BY4741,MATa; his3Δ 1; leu2Δ 0; met15Δ 0; ura3Δ; SWI4prD1scbmcb swi4::Swi4-GFPmut3-HIS3

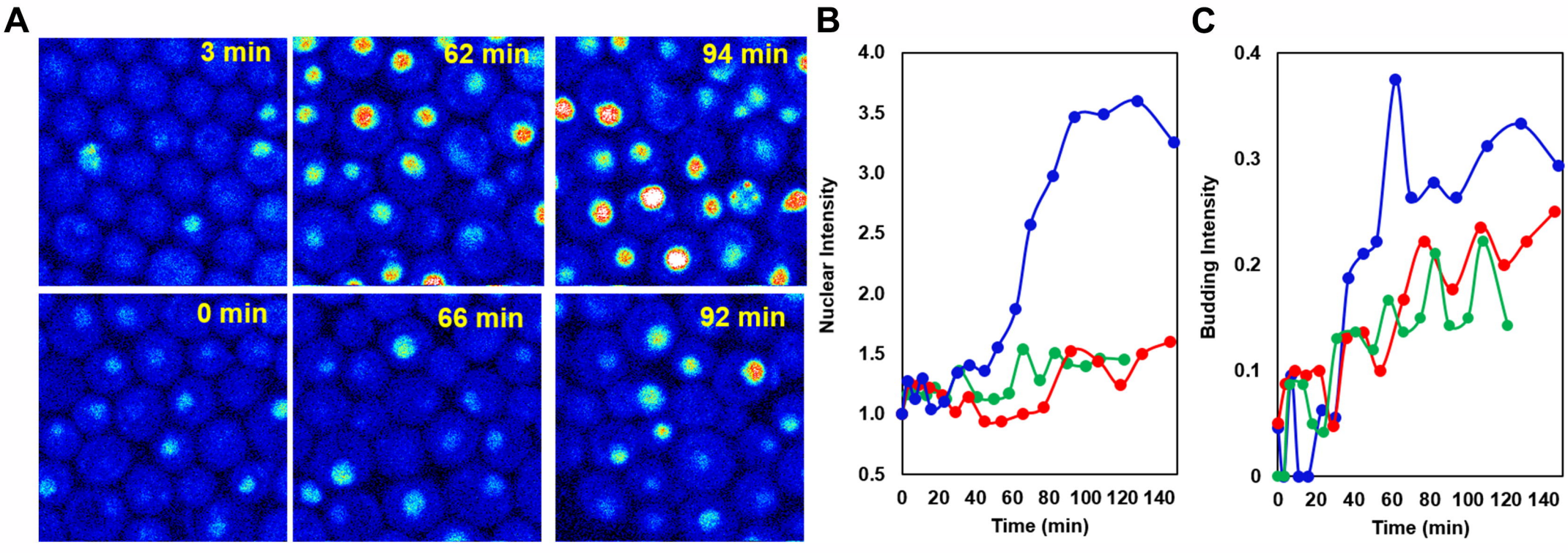
A
3 min
62 min
94 min
0 min
66 min
92 min
B
Nuclear Intensity
4.0
3.5
3.0
2.5
2.0
1.5
1.0
0.5
0 20 40 60 80 100 120 140
Time (min)
C
Budding Intensity
0.4
0.3
0.2
0.1
0
0 20 40 60 80 100 120 140
Time (min)

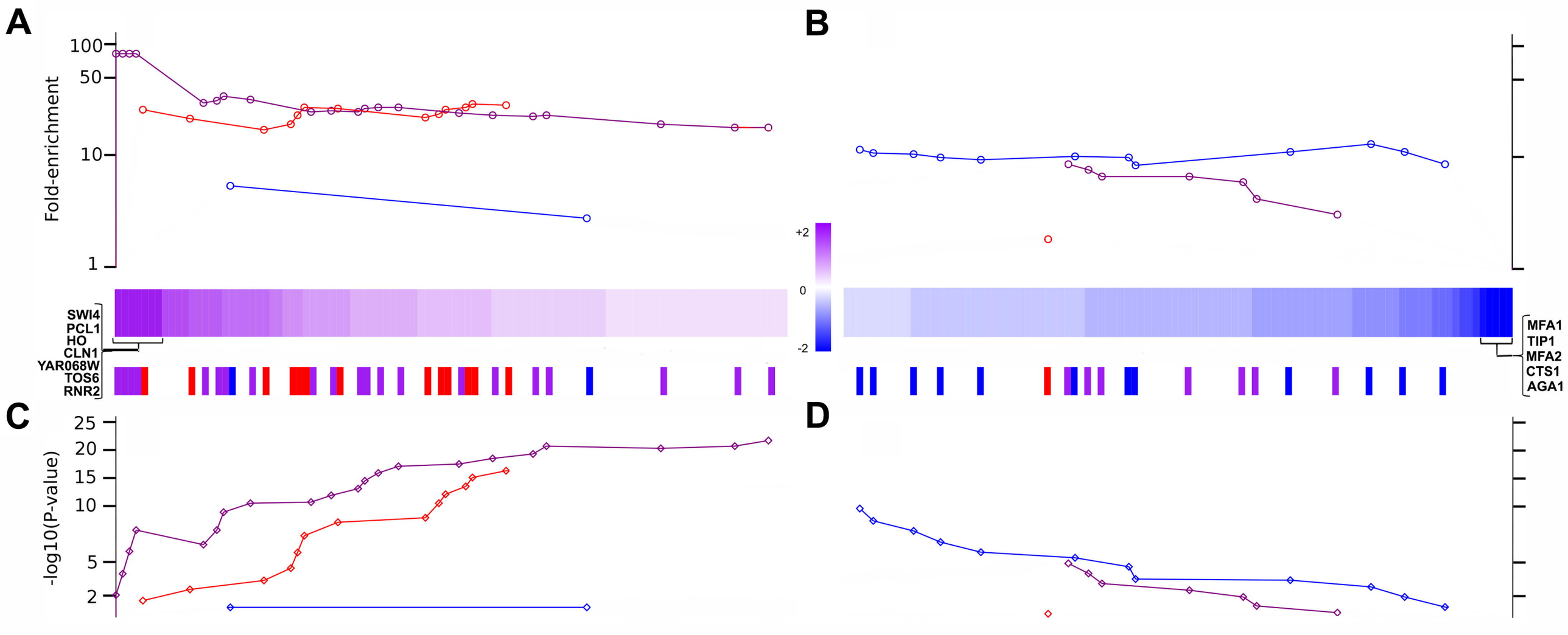
A
B
C
D
Fold-enrichment
100
50
10
1
-log10(P-value)
25
20
15
10
5
2
+2
0
-2
SWI4
PCL1
HO
CLN1
YAR068W
TOS6
RNR2
MFA1
TIP1
MFA2
CTS1
AGA1

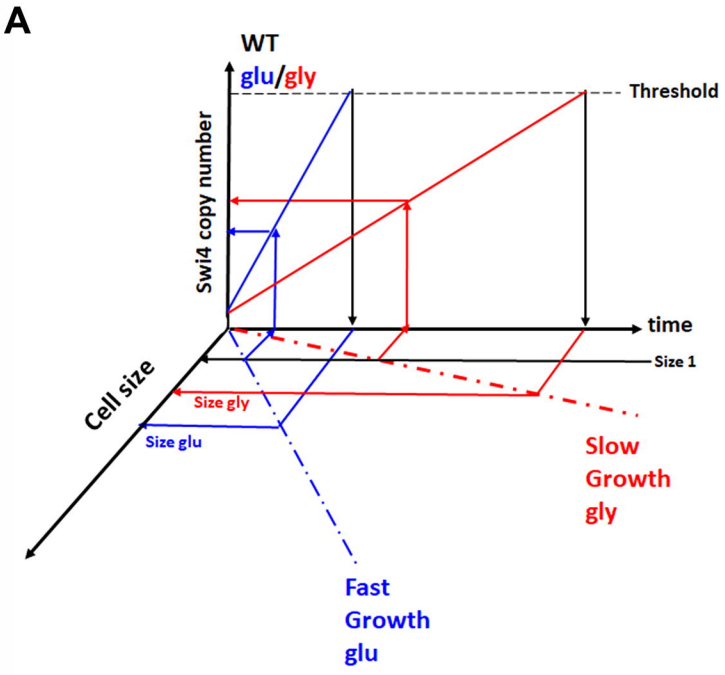
A
WT
glu/gly
Threshold
Swi4 copy number
time
Size 1
Cell size
Size gly
Size glu
Slow
Growth
gly
Fast
Growth
glu

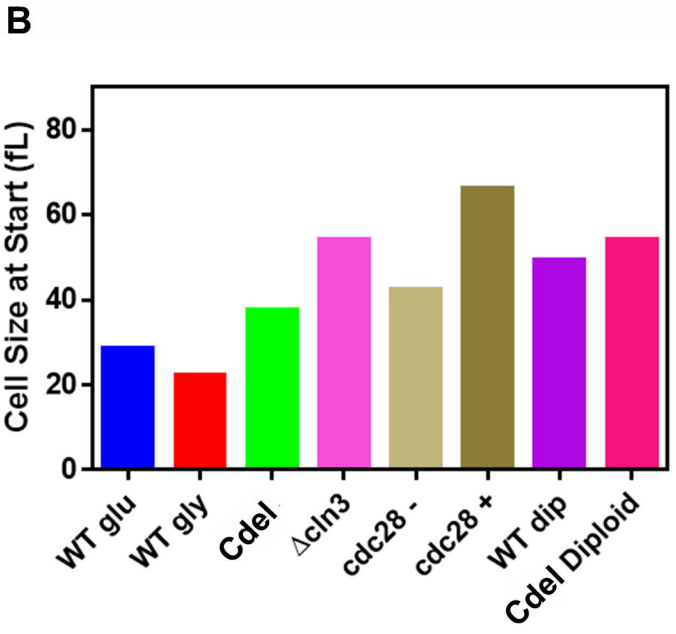
B
Cell Size at Start (fL)
0
20
40
60
80
WT glu
WT gly
Cdel
Δcln3
cdc28 -
cdc28 +
WT dip
Cdel Diploid

A

U

SCB1

cagtcatcgct

GTCTATGATACTACGATTTCACGAAAGAAAGCTGCAATAATTGAACATCATTGCTACTCCGTAAAACATGATAGTAAGAGTGCTTATCACGTGACACGTGTGCGGCAAATTTCGTAATTGATGATCAAAA 130

CAGATACTATGATGCTAAAGTGCTTTCTTTCGACGTTATTAACTTGTAGTAACGATGAGGCATTTTGTACTATCATTCTCACGAATAGTGCACTGTGCACACGCCGTTTAAAGCATTAACTACTAGTTTT

C

MCB1 MCB2 SCB2 ECB

tcagtgacGAAcaagtggatCACTAACCATGgacctcagatt

TATGGATACAATTACCTTCGGCGGCTAAAAACAACTTGATTTTGTTACCCGCGTTTGAAGTGACGCGTCACTAACCATGACGCGAAAGTTAATTATATTCAGCTCCCCGCCTGCTTATTTCCCGTTTAGG 780

ATACCTATGTTAATGGAAGCCGCCGATTTTTGTTGAACTAAAACAATGGGCGCAAACTTCACTGCGCAGTGATTGGTACTGCGCTTTCAATTAATATAAGTCGAGGGGCGGACGAATAAAGGGCAAATCC

AAATAAATGGTTAACCTAACAAAAAAAAAGAGGAACAAGGACTAAGAAGCACGTCAACGTGAAAAACGCACAAAAGATATTATAGTTATTGCCATCCTTTAGCATTGGTTTAGCATATCAACTAATTGA 910

TTTATTTACCAATTGGATTGTTTTTTTTTCTCCTTGTTCCTGATTCTTCGTGCAGTTGCACTTTTTGCGTGTTTTCTATAATATCAATAACGGTAGGAAATCGTAACCAAATCGTATAGTTGATTAACT

D

SCB3

acctagg

CTAATATTTGCTGCTAAATTCAACTGGAAGCTTTTTTTTTTTTCGAGATAATAAAAAAAGAAACTCTTTAGTGTATTGTGTTATTTTTACTATTAATTGTTGTTACAGCAGAATCACATCTAGCATTGGT 1040

GATTATAAACGACGATTTAAGTTGACCTTCGAAAAAAAAAAAAGCTCTATTATTTTTTTCTTTGAGAAATCACATAACACAATAAAAATGATAATTAACAACAATGTCGTCTTAGTGTAGATCGTAACCA

CGTCGCTTTTTCAAACGATTCTTCCTCCACTTACCCTTTGAAAAAAAGGTACATTATTTCACGTTATTTGATATATTGTCAACAATAATTGCTCTTTGCCGAAAATTAACTCTTCTTTCTTTCTCATTTC 1170

GCAGCGAAAAAGTTTGCTAAGAAGGAGGTGAATGGGAAACTTTTTTTCCATGTAATAAAGTGCAATAAACTATATAACAGTTGTTATTAACGAGAAACGGCTTTTAATTGAGAAGAAAGAAAGAGTAAAG

CCTTCTGTCCCTCTTGCGTAGTTCTAAAAGGTTGATTTATTCGAGAAATCATGCCATTTGATGTTTTGATATCAAACCAAAAAGATAATACCAATCACCAGAACATCACGCCAATATCAAAATCAGTTCT 1300

GGAAGACAGGGAGAACGCATCAAGATTTTCCAACTAAATAAGCTCTTTAGTACGGTAAACTACAAAACTATAGTTTGGTTTTTCTATTATGGTTAGTGGTCTTGTAGTGCGGTTATAGTTTTAGTCAAGA

M P F D V L I S N Q K D N T N H Q N I T P I S K S V L

B

Upstream (U) Central (C) Downstream (D)

SCB1 MCB1 MCB2 SCB2 ECB SCB3 SWI4 ORF

C delete
C mutations
C+D mutations
C+D+U mutations

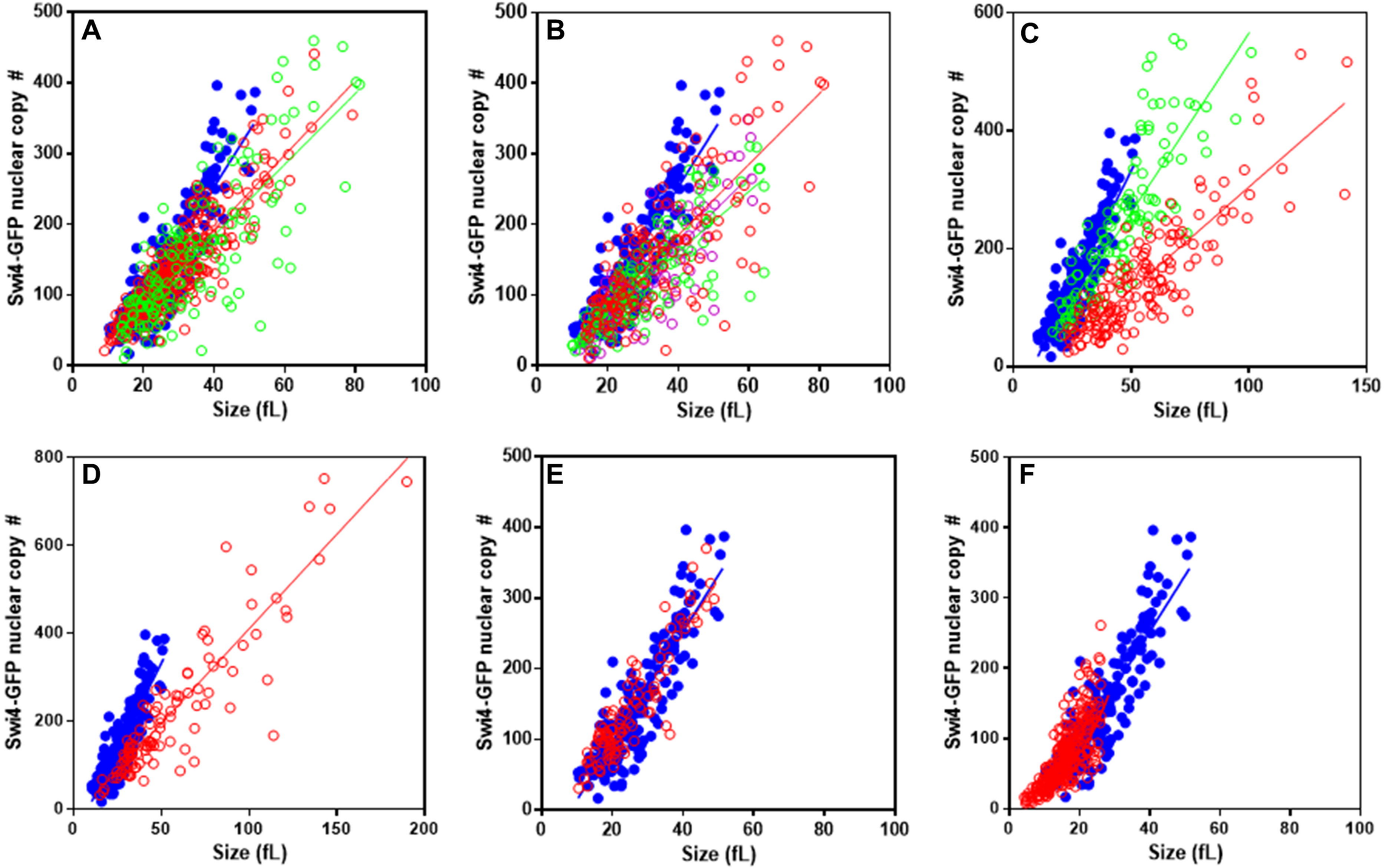
A
B
C
D
E
F
Swi4-GFP nuclear copy #
Size (fL)

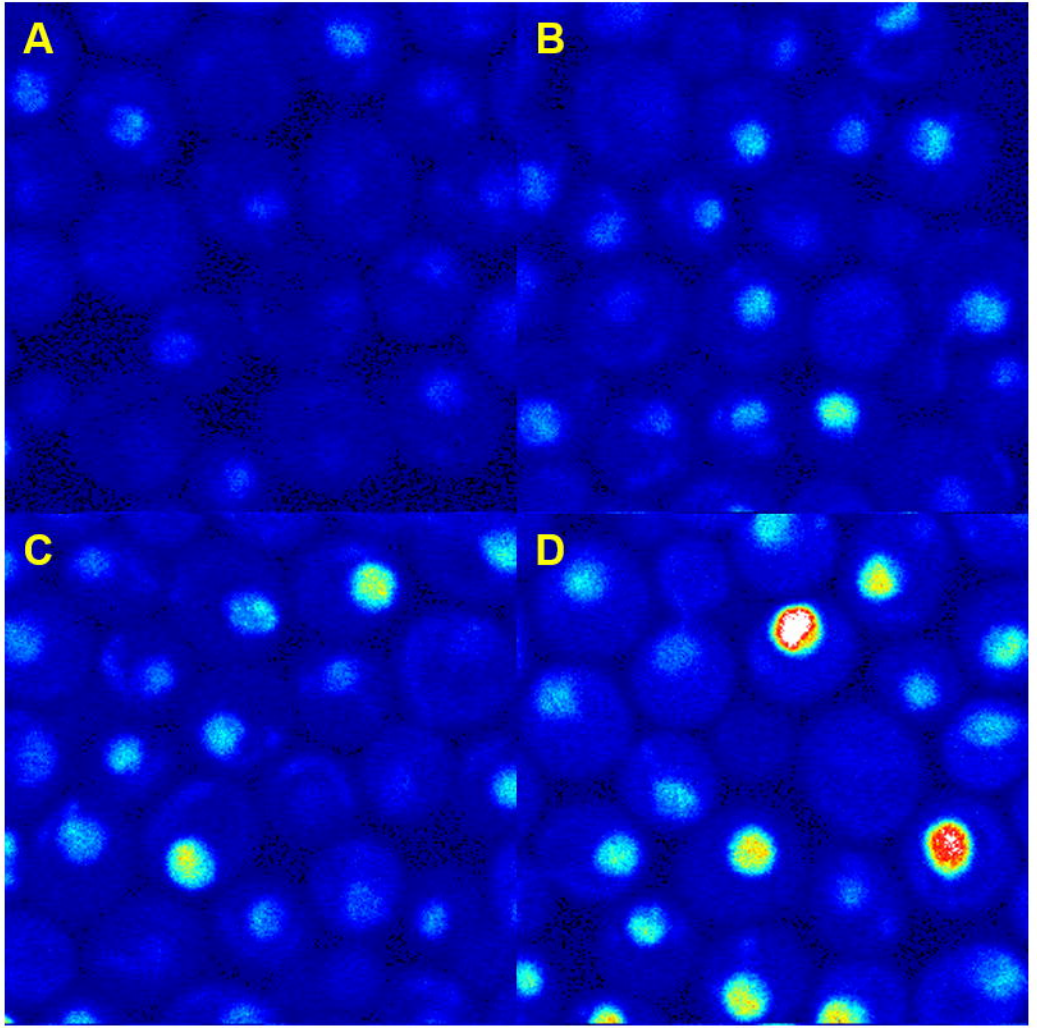
A
B
C
D

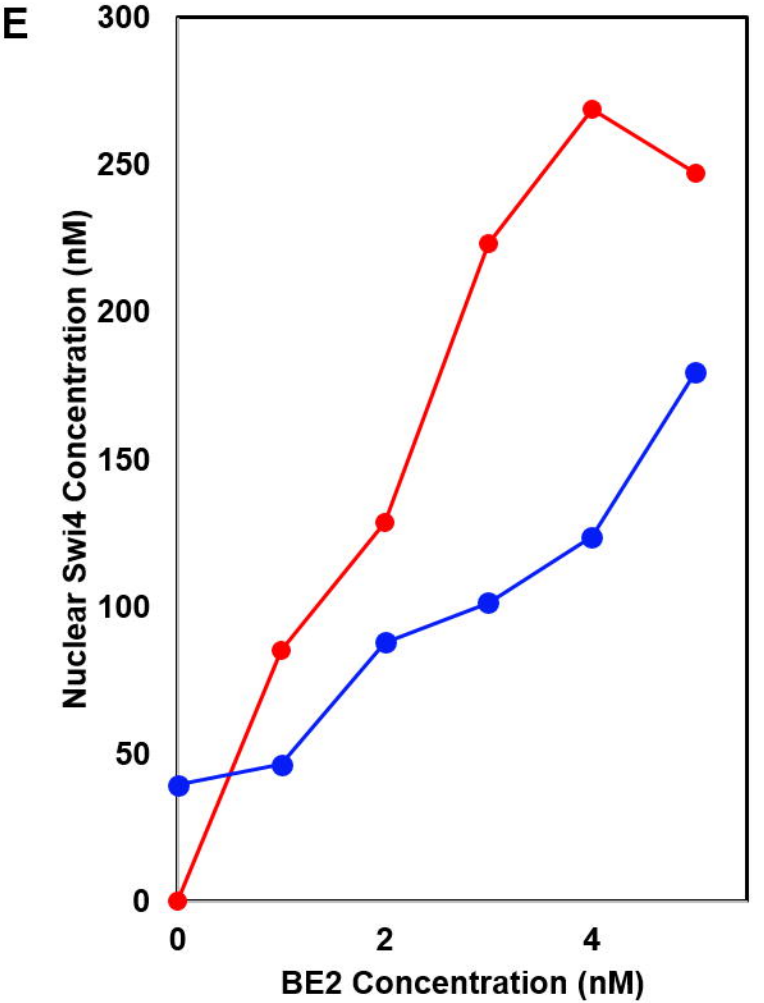
E
300
250
200
150
100
50
0
Nuclear Swi4 Concentration (nM)
0
2
4
BE2 Concentration (nM)